CMS Physics Analysis Summary

Contact: cms-pag-conveners-higgs@cern.ch 2014/07/03

Precise determination of the mass of the Higgs boson and studies of the compatibility of its couplings with the standard model

The CMS Collaboration

Abstract

Properties of the Higgs boson with mass near 125 GeV are measured in proton-proton collisions with the CMS experiment at the LHC. A comprehensive set of production and decay measurements are combined. The decays to $\gamma\gamma$, ZZ, WW, $\tau\tau$, and bb pairs are exploited, including studies targeting Higgs bosons produced in association with a pair of top quarks. The data samples were collected in 2011 and 2012 and correspond to integrated luminosities of up to 5.1 fb^{-1} at 7 TeV and up to 19.7 fb^{-1} at 8 TeV; the final detector calibration and alignment are used in the event reconstruction. From the high-resolution $\gamma\gamma$ and ZZ channels, the mass of this Higgs boson is measured to be $125.03\,^{+0.26}_{-0.27}$ (stat.) $^{+0.13}_{-0.15}$ (syst.) GeV, with the precision dominated by the statistical uncertainty. For this mass, the event yields obtained in the different analyses tagging specific decay modes and production mechanisms are consistent with those expected for the standard model Higgs boson. The combined best-fit signal strength, relative to the standard model expectation, is found to be $1.00 \pm 0.09\,\text{(stat.)}\,^{+0.08}_{-0.07}\,\text{(theo.)} \pm 0.07\,\text{(syst.)}$ at the measured mass. Various searches for deviations in the magnitudes of the Higgs boson scalar couplings from those predicted for the standard model are performed. No significant deviations are found.

1 Introduction

One of the most important objectives of the Large Hadron Collider (LHC) physics program is to understand the mechanism behind electroweak symmetry breaking (EWSB). In the standard model (SM) [1–3] EWSB is achieved by a complex scalar doublet field that leads to the prediction of one physical Higgs boson (H) [4–9].

In 2012 the ATLAS and CMS Collaborations at the LHC reported the observation of a new boson with a mass near 125 GeV [10–13]. Subsequent studies of the production and decay rates [14–24] and of the spin-parity quantum numbers [17, 18, 25, 26] of the new boson show that its properties are compatible with those expected for the SM Higgs boson.

In proton-proton (pp) collisions at $\sqrt{s} = 7$–8 TeV there are four main Higgs boson production mechanisms predicted by the SM. The gluon-gluon fusion production mode (ggH) has the largest cross section. It is followed by vector boson fusion (VBF), associated WH and ZH production (VH), and production in association with top quarks ($\mathrm{t\bar{t}H}$). The cross section values for the Higgs boson production modes and the values for the decay branching fractions, together with their uncertainties, are tabulated in Ref. [27] and references therein. For a Higgs boson mass between 124 GeV and 127 GeV, the total production cross section varies from 17.6 pb to 16.2 pb at $\sqrt{s} = 7$ TeV, and from 22.4 pb to 21.4 pb at 8 TeV.

The present combination uses the CMS measurements of the properties of this boson targeting its decay to bb [16], WW [17], ZZ [18], $\tau\tau$ [19], and $\gamma\gamma$ [20], as well as measurements of the $\mathrm{t\bar{t}H}$ production mode [14, 28, 29]. For simplicity, bb is used to denote $\mathrm{b\bar{b}}$, $\tau\tau$ to denote $\tau^+\tau^-$, etc. Similarly, ZZ is used to denote $\mathrm{ZZ}^{(*)}$ and WW to denote $\mathrm{WW}^{(*)}$.

The $\mathrm{H} \to \gamma\gamma$ and $\mathrm{H} \to \mathrm{ZZ}^{(*)} \to 4\ell$ (where $\ell = \mathrm{e}, \mu$) channels play a special role because of the excellent mass resolution of the reconstructed diphoton and four-lepton final states, respectively. The $\mathrm{H} \to \mathrm{WW}^{(*)} \to \ell\nu\ell\nu$ measurement has a high sensitivity but relatively poor mass resolution because of the presence of neutrinos in the final state. The bb and $\tau\tau$ decay modes are afflicted by large background contributions and have relatively poor mass resolution, making it challenging to obtain a sensitivity comparable to that of the other channels; combining the results from bb and $\tau\tau$, the CMS Collaboration has published evidence for the decay of this Higgs boson to fermions [30]. While in the SM the ggH process is dominated by (virtual) top-quark loops, directly probing the coupling of top quarks to this Higgs boson can be achieved by studying events tagged as having been produced via the $\mathrm{t\bar{t}H}$ process.

The mass of the new boson is determined by combining the published measurements of the $\mathrm{H} \to \gamma\gamma$ and $\mathrm{H} \to \mathrm{ZZ}^{(*)} \to 4\ell$ channels [18, 20]. The SM Higgs boson is predicted to have spin-parity quantum numbers $J^P = 0^+$, and all other properties can be derived if the boson's mass is specified. For the couplings of the Higgs boson to SM particles, we use the combination of all measurements to extract ratios between the observed coupling strengths and those predicted by the SM. The formalism used to test for deviations in the magnitudes of the Higgs boson scalar couplings is that set forth by the LHC Higgs Cross Section Working Group in Ref. [27] and references therein. This formalism assumes, among other things, that the observed state has $J^P = 0^+$ and that the narrow width approximation holds, leading to a factorization of the couplings in the production and decay of the boson.

The data sets have been processed with the final alignment and calibrations of the CMS detector [31] and correspond to pp collisions collected in 2011 and 2012 with integrated luminosities of up to 5.1 fb^{-1} at $\sqrt{s} = 7$ TeV and 19.7 fb^{-1} at 8 TeV. The central feature of the CMS detector is a 13 m long superconducting solenoid with an internal diameter of 6 m. The solenoid generates a uniform 3.8 T magnetic field parallel to the direction of the LHC beams. Within the

superconducting solenoid volume are a silicon pixel and strip tracker, a lead tungstate crystal electromagnetic calorimeter, and a brass/scintillator hadron calorimeter. Muons are identified and measured in gas-ionization detectors embedded in the outer steel magnetic flux return yoke of the solenoid. The detector is subdivided into a cylindrical barrel and endcap disks on either side. Calorimeters in the forward and backward directions complement the coverage provided by the barrel and endcap detectors.

In Section 2 the channels contributing to the combined measurements are summarized. In Section 3 the statistical method used to extract the boson properties is described; some expected differences between the results of the combination and those of the individual analyses are also explained. The results of the present combination are reported in Section 4.

2 Analyses entering the combination

Table 1 provides an overview of all analyses used in this combination, including the following information: the final states selected, the production and decay modes targeted by each analysis, the integrated luminosity used, the expected mass resolution, and the number of event categories in each channel.

The following notation is used in Table 1 and throughout the text: σ_{m_H}/m_H is the expected relative mass resolution, where σ_{m_H} is calculated differently in different input analyses; the $H \to \gamma\gamma$, $H \to ZZ^{(*)} \to 4\ell$, and $H \to WW^{(*)} \to \ell\nu\ell\nu$ analyses quote σ_{m_H} as half of the width of the shortest interval containing 68.3% of the signal events, while the $H \to \tau\tau$ analysis quotes the RMS of the signal distribution. Regarding leptons, ℓ denotes an electron or a muon, τ_h denotes a τ lepton identified via its decay into hadrons, and L denotes any charged lepton. Regarding lepton pairs, SF denotes same-flavor dileptons and SS (OS) denotes same-sign (opposite-sign) dileptons. Concerning reconstructed jets, CJV denotes a central jet veto, E_T^{miss} refers to missing transverse energy, j stands for a reconstructed jet, and b denotes a jet tagged as due to the hadronization of a b quark.

In total, 207 categories are combined, and there are 2519 nuisance parameters corresponding to sources of uncertainty other than those arising from Poisson (counting) statistics.

2.1 $H \to \gamma\gamma$

The $H \to \gamma\gamma$ analysis [20] measures a narrow signal mass peak over a smoothly falling background due to events originating from prompt non-resonant diphoton production or from events with at least one jet misidentified as an isolated photon.

The sample of events with a photon pair is split in mutually exclusive event classes targeting the different production processes as listed in Table 1. Requiring the presence of two forward jets favors events produced by the VBF mechanism, while event classes designed to preferentially select VH or $t\bar{t}H$ production require the presence of muons, electrons, E_T^{miss}, a pair of jets compatible with the decay of a vector boson, or jets arising from the hadronization of b quarks. For 7 TeV data, there is only one $t\bar{t}H$-tagged event class that combines the events selected by the leptonic $t\bar{t}H$ and multijet $t\bar{t}H$ selections. The 2-jet VBF-tagged classes are further split according to a multivariate (MVA) classifier that is trained to discriminate VBF events from both background and ggH events.

Fewer than 1% of the selected events are tagged according to production mode. The remaining "untagged" events are subdivided into different classes based on the output of an MVA classifier that assigns a high score to signal-like events and to events with a good mass resolution,

Table 1: Summary of the channels in the analyses included in this combination. The first and second columns indicate which decay mode and/or production mechanism are targeted by an analysis. Notes on the expected composition of the signal are given in the third column. Where relevant, the fourth column specifies the expected relative mass resolution for the SM Higgs boson. Finally, the last columns provide the number of categories and the integrated luminosity for the 7 and 8 TeV data sets. The notation is explained in the text.

Decay tag and production tag		Expected signal composition	σ_{m_H}/m_H	*Luminosity (fb^{-1})* No. of categories	
				7 TeV	8 TeV
$H \to \gamma\gamma$ [20], Section 2.1				*5.1*	*19.7*
$\gamma\gamma$	Untagged	76–93% ggH	0.8–2.1%	4	5
	2-jet VBF	50–80% VBF	1.0–1.3%	2	3
	Leptonic VH	≈95% VH (WH/ZH ≈ 5)	1.3%	2	2
	E_T^{miss} VH	70–80% VH (WH/ZH ≈ 1)	1.3%	1	1
	2-jet VH	≈65% VH (WH/ZH ≈ 5)	1.0–1.3%	1	1
	Leptonic $t\bar{t}H$	≈95% $t\bar{t}H$	1.1%	1†	1
	Multijet $t\bar{t}H$	>90% $t\bar{t}H$	1.1%		1
$H \to ZZ^{(*)} \to 4\ell$ [18], Section 2.2				*5.1*	*19.7*
4μ, 2e2μ, 4e	2-jet	42% VBF + VH	1.3, 1.8, 2.2%‡	3	3
	Other	≈90% ggH		3	3
$H \to WW^{(*)} \to \ell\nu\ell\nu$ [17], Section 2.3				*4.9*	*19.4*
ee + $\mu\mu$, eμ	0-jet	96–98% ggH	eμ: 16%‡	2	2
	1-jet	82–84% ggH	eμ: 17%‡	2	2
	2-jet VBF	78–86% VBF		2	2
	2-jet VH	31–40% VH		2	2
$3\ell 3\nu$ WH	SF-SS, SF-OS	≈100% WH, up to 20% $\tau\tau$		2	2
$\ell\ell + \ell'\nu$jj ZH	eee, eeμ, $\mu\mu\mu$, $\mu\mu$e	≈100% ZH		4	4
$H \to \tau\tau$ [19], Section 2.4				*4.9*	*19.7*
eτ_h, $\mu\tau_h$	0-jet	≈98% ggH	11–14%	4	4
	1-jet	70–80% ggH	12–16%	5	5
	2-jet VBF	75–83% VBF	13–16%	2	4
$\tau_h\tau_h$	1-jet	67–70% ggH	10–12%	-	2
	2-jet VBF	80% VBF	11%	-	1
eμ	0-jet	≈98% ggH, 23–30% WW	16–20%	2	2
	1-jet	75–80% ggH, 31–38% WW	18–19%	2	2
	2-jet VBF	79–94% VBF, 37–45% WW	14–19%	1	2
ee, $\mu\mu$	0-jet	88–98% ggH		4	4
	1-jet	74–78% ggH, ≈17% WW ⋆		4	4
	2-jet CJV	≈50% VBF, ≈45% ggH, 17–24% WW ⋆		2	2
$\ell\ell + LL'$ ZH	$LL' = \tau_h\tau_h, \ell\tau_h$, e$\mu$	≈15% (70%) WW for $LL' = \ell\tau_h$ (eμ)		8	8
$\ell + \tau_h\tau_h$ WH		≈96% VH, ZH/WH ≈ 0.1		2	2
$\ell + \ell'\tau_h$ WH		ZH/WH ≈ 5%, 9–11% WW		2	4
VH with $H \to bb$ [16], Section 2.5				*5.1*	*18.9*
W($\ell\nu$)bb	p_T(V) bins	≈100% VH, 96–98% WH	≈10%	4	6
W($\tau_h\nu$)bb		93% WH		-	1
Z($\ell\ell$)bb	p_T(V) bins	≈100% ZH		4	4
Z($\nu\nu$)bb	p_T(V) bins	≈100% VH, 62–76% ZH		2	3
$t\bar{t}H$ with $H \to$ hadrons [14, 28], Section 2.6				*5.0*	*19.3*
$H \to bb$	$t\bar{t}$ lepton+jets	≈90% bb but ≈24% WW in ≥6j + 2b		7	7
	$t\bar{t}$ dilepton	45–85% bb, 8–35% WW, 4–14% $\tau\tau$		2	3
$H \to \tau_h\tau_h$	$t\bar{t}$ lepton+jets	68–80% $\tau\tau$, 13–22% WW, 5–13% bb		-	6
$t\bar{t}H$ with $H \to$ leptons [29], Section 2.6				-	*19.6*
2ℓ-SS		WW/$\tau\tau \approx 3$		-	6
3ℓ		WW/$\tau\tau \approx 3$		-	2
4ℓ		WW : $\tau\tau$: ZZ ≈ 3 : 2 : 1		-	1

† Events fulfilling the requirements of either selection are combined into one category.

‡ Values for analyses dedicated to the measurement of the mass that do not use the same categories and/or observables.

⋆ Composition in the regions for which the ratio between signal and background $s/(s+b) > 0.05$.

based on a combination of i) an event-by-event estimate of the diphoton mass resolution, ii) a photon identification score for each photon, and iii) kinematic information about the photons and the diphoton system. The photon identification score is obtained from a separate MVA classifier that uses shower shape information and variables characterizing how isolated the photon candidate is to discriminate prompt photons from those arising in jets.

In each event class, the background in the signal region is estimated from a fit to the observed diphoton mass distribution in data. The uncertainty due to the choice of background functional form is incorporated into the statistical procedure; the likelihood maximization is also performed for a discrete variable that selects which of the functional forms is evaluated. This procedure was found to have correct coverage probability and negligible bias in extensive tests using pseudo-data extracted from fits of multiple families of functional forms to the data. By construction, this "discrete profiling" of the background functional form leads to confidence intervals on any estimated parameter that are at least as large as those obtained when considering any single functional form. Parameters related to the background functional forms contribute to the statistical uncertainty of measurements.

Three cross-check analyses corroborate the main results. As an alternative to the use of MVA algorithms, an analysis using simpler selections but the same background treatment is performed. An analysis using sidebands is used to cross-check the background treatment. Finally, to cross-check the conclusions regarding VBF production, a two-dimensional analysis using the diphoton and dijet masses was developed.

The same event classes and observables are used for the mass measurement and to search for deviations in the magnitudes of the Higgs boson scalar couplings.

2.2 $H \to ZZ$

In the $H \to ZZ^{(*)} \to 4\ell$ analysis [18], we measure a four-lepton mass peak over a small continuum background. To further separate signal and background, we build a discriminant, $\mathcal{D}^{\text{kin}}_{\text{bkg}}$, using the leading order matrix elements for signal and background. The value of $\mathcal{D}^{\text{kin}}_{\text{bkg}}$ is calculated from the observed kinematics, namely the masses of the two dilepton pairs and five angles, which uniquely define a four-lepton configuration in their center-of-mass frame.

Given the different mass resolutions and different background rates arising from jets misidentified as leptons, the 4e, 4μ, and $2e2\mu$ event categories are analyzed separately.

The dominant irreducible background in this channel is due to non-resonant ZZ production with both Z bosons decaying to a pair of charged leptons and is estimated from simulation. The smaller reducible backgrounds with misidentified leptons, mainly from the production of $Z + \text{jets}$, $t\bar{t}$, and $WZ + \text{jets}$, are estimated from data.

To increase the sensitivity to the production mechanism, the event sample is split into two categories based on jet multiplicity: i) events with fewer than two jets, and ii) events with at least two jets. In the first category, the four-lepton transverse momentum is used to discriminate VBF and VH production from ggH. In the second category a linear discriminant, built from the invariant mass of the two leading jets and their pseudorapidity difference, is used to separate the VBF and ggH processes.

For the mass measurement an event-by-event estimator of the mass resolution is built from the single-lepton momentum resolutions evaluated from the study of a large number of $J/\psi \to \mu\mu$ and $Z \to \ell\ell$ data events. The relative mass resolution, $\sigma_{m_{4\ell}}/m_{4\ell}$, is then used together with $m_{4\ell}$ and $\mathcal{D}^{\text{kin}}_{\text{bkg}}$ to measure the boson mass.

2.3 $H \to WW$

In the $H \to WW^{(*)} \to \ell\nu\ell\nu$ analysis [17], we measure an excess of events with two oppositely-charged leptons or three leptons with a total charge of ± 1, moderate E_T^{miss}, and up to two jets.

The two-lepton events are divided into six categories, with different background compositions and signal-to-background ratios. For events with no jets, the main background is due to non-resonant WW production; for events with one jet, the dominant backgrounds are from WW and top-quark production. The events are split into same-flavor and different-flavor dilepton event categories, since the background from Drell–Yan production ($qq \to \gamma^*/Z^{(*)} \to \ell\ell$) is much larger for same-flavor dilepton events. The 2-jet VBF tags are optimized to take advantage of the VBF production signature. The main background is from top-quark production. The 2-jet VH tag targets the decay of the vector boson into two jets, $V \to jj$. The selection requires two centrally-produced jets with invariant mass in the range $65 < m_{jj} < 105\,\text{GeV}$. To reduce the top-quark, Drell–Yan, and WW backgrounds, a selection is performed on the dilepton mass and on the angular separation between the leptons. All background rates, except for very small contributions from WW, ZZ, and $W\gamma$, are evaluated from data. The two-dimensional distribution of events in the $(m_{\ell\ell}, m_T)$ plane, where $m_{\ell\ell}$ is the invariant mass of the dilepton pair and m_T is the transverse mass reconstructed from the transverse momentum of the dilepton pair and the E_T^{miss} vector, is used for the measurements in the different-flavor dilepton categories with zero and one jets. For the same-flavor dilepton categories and for the 2-jet VH tag analysis only the event totals are used.

In the $3\ell 3\nu$ channel tagging $WH \to WWW$, we search for an excess of events with three leptons, electrons or muons, large E_T^{miss}, and low hadronic activity. The dominant background is from $WZ \to 3\ell\nu$ production, which is largely reduced by requiring that all same-flavor and oppositely-charged lepton pairs have a dilepton mass away from the Z boson mass. The smallest distance between the oppositely-charged leptons is the observable chosen to perform the measurement. The background processes with jets misidentified as leptons, e.g., $Z + \text{jets}$ and top production, as well as the $WZ \to 3\ell\nu$ background are estimated from data. The small contribution from the $ZZ \to 4\ell$ process with one of the leptons having escaped detection is estimated using simulated samples.

In the $3\ell\nu jj$ channel targeting $ZH \to Z + WW \to \ell\ell + \ell\nu jj$, we first identify the leptonic decay of the Z boson and then require the dijet system to satisfy $|m_{jj} - m_W| \leq 60\,\text{GeV}$. The transverse mass of the $\ell\nu jj$ system is the observable chosen to perform the measurement. The main backgrounds are due to the production of WZ, ZZ, and tri-bosons, as well as processes involving non-prompt leptons. The first three are estimated from simulated samples, while the last one is evaluated from data. It should be noted that in the $3\ell 3\nu$ channel up to 20% of the decays are due to $H \to \tau\tau$. This contribution is negligible in the $3\ell\nu jj$ channel.

Finally, a dedicated analysis for the measurement of the mass is performed in the 0-jet and 1-jet categories of the $e\mu$ channel. Employing observables which are extensively used in SUSY searches, a resolution of 16–17% for $m_H = 125\,\text{GeV}$ has been achieved.

2.4 $H \to \tau\tau$

The $H \to \tau\tau$ analysis [19] measures an excess of events using multiple final-state signatures including the $e\mu$, $e\tau_h$, $\mu\tau_h$, and $\tau_h\tau_h$ final states, where electrons and muons arise from leptonic τ decays. The samples are further divided into categories based on the number of reconstructed jets in the event: 0 jets, 1 jet, or 2 jets. The 0-jet and 1-jet categories are further subdivided according to the reconstructed p_T of the leptons. The 2-jet categories require a VBF-like topology

and are subdivided according to selection criteria applied to the dijet kinematic properties. In each of these categories, we search for a broad excess in the reconstructed $\tau\tau$ mass distribution. The 0-jet category is used to constrain background normalizations, identification efficiencies, and energy scales. Various control samples in data are used to evaluate the main irreducible background from $Z \to \tau\tau$ production and the largest reducible backgrounds from $W + \text{jets}$ and multijet production.

The ee and $\mu\mu$ final states are similarly subdivided into categories as above but given the two neutrinos present in the final state the search is performed on the combination of two MVA discriminants. The first is trained to distinguish $Z \to \ell\ell$ events from $Z \to \tau\tau$ events while the second is trained to separate $Z \to \tau\tau$ events from $H \to \tau\tau$ events.

The search for $H \to \tau\tau$ decays produced in association with a W or Z boson is conducted in events with three or four leptons in the final state. The analysis targeting WH production selects events that have electrons or muons and one or two hadronically-decaying tau leptons: $\mu + \mu\tau_h$, $e + \mu\tau_h$ or $\mu + e\tau_h$, $\mu + \tau_h\tau_h$, and $e + \tau_h\tau_h$. The analysis targeting ZH production selects events with an identified $Z \to \ell\ell$ decay and a Higgs boson candidate decaying to $e\mu$, $e\tau_h$, $\mu\tau_h$, or $\tau_h\tau_h$. The main irreducible backgrounds to the WH and ZH searches are WZ and ZZ diboson events, respectively. The irreducible backgrounds are estimated using simulated event samples corrected by measurements from control samples in data. The reducible backgrounds in both analyses are W, Z, and $t\bar{t}$ events with at least one jet misidentified as an isolated e, μ, or τ_h. These backgrounds are estimated exclusively from data by measuring the probability for jets to be misidentified as isolated leptons in background-enriched control regions, and weighting the selected events that fail the lepton requirements with the misidentification probability. For the SM Higgs boson, the expected fraction of $H \to WW$ events in the ZH analysis is 10–15% for $ZH \to Z + \ell\tau_h$ and 70% for $ZH \to Z + e\mu$.

2.5 VH with $H \to bb$

Exploiting the large expected $H \to bb$ branching fraction, the analysis of VH production and $H \to bb$ decay examines the $W(\ell\nu)bb$, $W(\tau_h\nu)bb$, $Z(\ell\ell)bb$, and $Z(\nu\nu)bb$ topologies [16].

The Higgs boson candidate is reconstructed by requiring two b-tagged jets. The event sample is divided into classes depending on the transverse momentum of the vector boson, $p_T(V)$. An MVA regression is used to estimate the true b-quark energy after being trained on reconstructed b-jets in simulated $H \to bb$ events. This regression achieves a final dijet mass resolution of about 10% for $m_H = 125\,\text{GeV}$. The performance of the regression algorithm is checked with data where it is observed to improve the top-quark mass measurement in $t\bar{t}$ events and to improve the p_T balance between a Z boson and b-quark jets in $Z(\to \ell\ell) + bb$ events. Events with higher $p_T(V)$ have smaller backgrounds and better dijet mass resolution. A cascade of MVA classifiers, trained to distinguish the signal from $t\bar{t}$, $V + \text{jets}$, and diboson events, improves the sensitivity in the $W(\ell\nu)bb$, $W(\tau_h\nu)bb$, and $Z(\nu\nu)bb$ channels. The rates of the main backgrounds, consisting of $V + \text{jets}$ and $t\bar{t}$ events, are derived from signal-depleted data control samples. The WZ and ZZ backgrounds where $Z \to bb$, as well as the single-top-quark background, are estimated from simulated samples. The MVA classifier output distribution is used as the final discriminant in performing measurements.

2.6 $t\bar{t}H$-production analyses

Given its distinctive signature, the $t\bar{t}H$ production process can be tagged using the decay products of the $t\bar{t}$ pair. The search for $t\bar{t}H$ production is performed in three channels: $H \to bb$ [28], $H \to \tau_h\tau_h$ [28], and $H \to$ leptons [29].

In the analysis of $t\bar{t}H$ production with $H \to bb$, two signatures for the $t\bar{t}$ pair decay are considered: lepton-plus-jets ($t\bar{t} \to \ell\nu jjbb$) and dilepton ($t\bar{t} \to \ell\nu\ell\nu bb$). In the analysis of $t\bar{t}H$ production with $H \to \tau_h\tau_h$, the $t\bar{t}$ lepton-plus-jets decay signature is required. In both channels, the events are further classified according to the numbers of jets and b-tagged jets identified. The major background is from top-pair production accompanied by extra jets. An MVA is trained to discriminate between background and signal events using information related to reconstructed object kinematics, event shape, and the discriminant output from the b-quark-jet tagging algorithm. The rates of background processes are estimated from simulated samples and are constrained through the inclusion of background enriched control samples in the statistical procedure.

The analysis of $t\bar{t}H$ production and $H \to$ leptons is mainly sensitive to the Higgs decays to WW, $\tau\tau$, and ZZ, with subsequent decay to electrons and/or muons. The selection starts by requiring the presence of at least two central jets and at least one jet tagged as originating from a b quark. It then proceeds to categorize the events depending on the number, charge, and flavor of the reconstructed leptons: 2ℓ with the same sign, 3ℓ with a total charge of ± 1, or 4ℓ. A dedicated MVA lepton selection is used to suppress the reducible background from misidentified leptons, usually from the decay of b hadrons. After the final selection, the two main backgrounds include one that is due to misidentified leptons, which is evaluated from data, and associated production of $t\bar{t}$ and vector bosons, which is estimated from simulated samples. Measurements in the 4ℓ event category are performed using the number of reconstructed jets, N_j. In the remaining categories an MVA classifier is employed, which makes use of N_j as well as other kinematic and event shape variables to discriminate between signal and background.

3 Combination methodology

The combination of Higgs boson measurements requires the simultaneous analysis of the data selected by all individual analyses, accounting for all statistical uncertainties, systematic uncertainties, and their correlations.

The overall statistical methodology used in this combination was developed by the ATLAS and CMS Collaborations in the context of the LHC Higgs Combination Group and is described in Refs. [12, 32, 33]. The chosen test statistic q is based on the profile likelihood ratio and is used to determine how signal-like or background-like the data are. Systematic uncertainties are incorporated in the analysis via nuisance parameters that are treated according to the frequentist paradigm. Below we give concise definitions of statistical quantities that we use for characterizing the outcome of the measurements. Results presented in this note are obtained using asymptotic formulae [34], including a few updates recently introduced in the RooStats package [35].

3.1 Characterizing an excess of events: p-values and significance

To quantify the presence of an excess of events over what is expected for the background, we use the test statistic where the likelihood appearing in the numerator corresponds to the background-only hypothesis:

$$q_0 \;=\; -2\,\ln\frac{\mathcal{L}(\text{data}\,|\,b,\,\hat{\theta}_0)}{\mathcal{L}(\text{data}\,|\,\hat{\mu}\cdot s+b,\,\hat{\theta})},\ \text{with}\ \hat{\mu}>0, \tag{1}$$

where s stands for the signal expected under the SM Higgs hypothesis, μ is a signal strength

modifier introduced to accommodate deviations from SM Higgs predictions, b stands for backgrounds, and θ are nuisance parameters describing systematic uncertainties. The value $\hat{\hat{\theta}}_0$ maximizes the likelihood in the numerator under the background-only hypothesis, $\mu = 0$, while $\hat{\mu}$ and $\hat{\theta}$ define the point at which the likelihood reaches its global maximum.

The quantity p_0, henceforth referred to as the local p-value, is defined as the probability, under the background-only (b) hypothesis, to obtain a value q_0 at least as large as that observed in data, q_0^{data}:

$$p_0 = \mathrm{P}\left(q_0 \geq q_0^{\text{data}} \,\middle|\, b\right). \tag{2}$$

The local significance z of a signal-like excess is then computed from the following equation, using the one-sided Gaussian tail convention:

$$p_0 \;=\; \int_z^{+\infty} \frac{1}{\sqrt{2\pi}} \exp(-x^2/2)\; dx. \tag{3}$$

Note that very small p-values should be interpreted with caution as the systematic biases and uncertainties in the underlying model are only known with finite precision.

3.2 Extracting signal model parameters

Signal model parameters a, such as the signal strength modifier μ, are evaluated from scans of the profile likelihood ratio $q(a)$:

$$q(a) \;=\; -2\,\Delta \ln \mathcal{L} \;=\; -2\,\ln \frac{\mathcal{L}(\text{data} \,|\, s(a) + b,\, \hat{\hat{\theta}}_a)}{\mathcal{L}(\text{data} \,|\, s(\hat{a}) + b,\, \hat{\theta})}. \tag{4}$$

The parameters $\hat{a}$ and $\hat{\theta}$ correspond to the global maximum likelihood and are called the best-fit set.

The post-fit model, obtained after the signal-plus-background fit to the data, corresponds to the parametric bootstrap described in the statistics literature, includes information gained in the fit regarding the values of all parameters [36, 37], and is used when deriving expected quantities.

The 68% and 95% confidence level (CL) intervals for a given parameter of interest a_i are evaluated from $q(a_i) = 1.00$ and $q(a_i) = 3.84$ respectively, with all other unconstrained model parameters treated in the same way as the nuisance parameters. The two-dimensional (2D) 68% and 95% CL contours for pairs of parameters are derived from $q(a_i, a_j) = 2.30$ and $q(a_i, a_j) = 6.99$, respectively. One should keep in mind that boundaries of 2D confidence regions projected on either parameter axis are not identical to the one-dimensional (1D) confidence interval for that parameter.

All results are given using the chosen test statistic result in approximate CL intervals or regions.

3.3 Grouping of channels by decay tag and by production tag

The event samples selected by the different analyses are mutually exclusive. The selection criteria can, in most cases, define pure selections of the targeted decay or production modes. For instance, the $\mathrm{t\bar{t}H}$-tagged event classes of the $\mathrm{H} \to \gamma\gamma$ analysis are pure in terms of $\gamma\gamma$ decays and are expected to contain less than 10% of non-$\mathrm{t\bar{t}H}$ events.

Unfortunately, in some cases such pure compositions are not achievable for both production and decay tags. Mixed production mode composition is common in VBF-tagged event classes where the ggH contribution can be as high as 50%, or in VH tags where WH and ZH mixtures are common. On the decay side, mixed composition is more marked for signatures involving light leptons and $E_{\mathrm{T}}^{\mathrm{miss}}$, where both the $\mathrm{H} \to \mathrm{WW}$ and $\mathrm{H} \to \tau\tau$ decays may contribute. This can be seen in Table 1, where some VH-tag analyses targeting $\mathrm{H} \to \mathrm{WW}$ decays have a significant contribution from $\mathrm{H} \to \tau\tau$ decays and vice versa. This is also the case of the $\mathrm{e}\mu$ channel in the $\mathrm{H} \to \tau\tau$ analysis, in particular in the 2-jet VBF tag categories, where the contribution from $\mathrm{H} \to \mathrm{WW}$ decays is sizable and concentrated at low values of $m_{\tau\tau}$, entailing a genuine sensitivity of these categories to $\mathrm{H} \to \mathrm{WW}$ decays. On the other hand, in the ee and $\mu\mu$ channels of the $\mathrm{H} \to \tau\tau$ analysis, the contribution from $\mathrm{H} \to \mathrm{WW}$ is large when integrated over the full range of the MVA observable used, but given that the analysis was optimized for $\tau\tau$ decays the contribution from $\mathrm{H} \to \mathrm{WW}$ is not concentrated in the regions with largest signal-to-background ratio, and provides little added sensitivity.

Another case of mixed decay composition is that of the analyses targeting $\mathrm{t\bar{t}H}$ production, where the $\mathrm{H} \to$ leptons decay selection includes sizable contributions from $\mathrm{H} \to \mathrm{WW}$ and $\mathrm{H} \to \tau\tau$ decays, and to a lesser extent also from $\mathrm{H} \to \mathrm{ZZ}$ decays. The mixed composition is a consequence of designing the analysis to have the highest possible sensitivity to the $\mathrm{t\bar{t}H}$ production mode. The analysis of $\mathrm{t\bar{t}H}$ with $\mathrm{H} \to \tau_{\mathrm{h}}\tau_{\mathrm{h}}$ decay has a composition that is dominated by $\mathrm{H} \to \tau\tau$ decays, followed by $\mathrm{H} \to \mathrm{WW}$ decays, and a smaller contribution of $\mathrm{H} \to \mathrm{bb}$ decays. Finally, in the analysis of $\mathrm{t\bar{t}H}$ with $\mathrm{H} \to \mathrm{bb}$, there is an event class of the lepton + jets channel that requires six or more jets and two b-tagged jets where the signal is expected to be 58% from $\mathrm{H} \to \mathrm{bb}$, 24% from $\mathrm{H} \to \mathrm{WW}$, and the remaining 18% from the other SM decay modes; in the dilepton channel, the event class requiring four or more jets and two b-tagged jets is expected to contain 45% from $\mathrm{H} \to \mathrm{bb}$, 35% from $\mathrm{H} \to \mathrm{WW}$, and 14% from $\mathrm{H} \to \tau\tau$.

When results are grouped according to decay tag, each individual category is assigned to the decay mode group that, in the SM, is expected to dominate the sensitivity in that channel. In particular,

$\mathrm{H} \to \gamma\gamma$ **tagged** includes only categories from the $\mathrm{H} \to \gamma\gamma$ analysis of Ref. [20].

$\mathrm{H} \to \mathrm{ZZ}$ **tagged** includes only categories from the $\mathrm{H} \to \mathrm{ZZ}$ analysis of Ref. [18].

$\mathrm{H} \to \mathrm{WW}$ **tagged** includes all the channels from the $\mathrm{H} \to \mathrm{WW}$ analysis of Ref. [17] and the channels from the analysis of $\mathrm{t\bar{t}H}$ with $\mathrm{H} \to$ leptons of Ref. [29].

$\mathrm{H} \to \tau\tau$ **tagged** includes all the channels from the $\mathrm{H} \to \tau\tau$ analysis of Ref. [19] and the channels from the analysis of $\mathrm{t\bar{t}H}$ targeting $\mathrm{H} \to \tau_{\mathrm{h}}\tau_{\mathrm{h}}$ of Ref. [28].

$\mathrm{H} \to \mathrm{bb}$ **tagged** includes all the channels of the analysis of VH with $\mathrm{H} \to \mathrm{bb}$ of Ref. [16] and the channels from the analysis of $\mathrm{t\bar{t}H}$ targeting $\mathrm{H} \to \mathrm{bb}$ of Refs. [14, 28].

When results are grouped by production tag, the same reasoning of assignment by preponderance of composition is followed, using the information in Table 1.

3.4 Expected differences with respect to the results of input analyses

The grouping of channels described in Section 3.3 is among the reasons why the results of the combination may differ from those of the individual published analyses. In addition, the combined measurement takes into account correlations among several sources of systematic

uncertainty. Care is taken to understand the post-fit behavior of the parameters that are correlated between analyses. Finally, the combination is evaluated at a value of m_{H} that is not the value that has been used in some of the individual published analyses, entailing changes to the expected cross section and branching fractions for the SM Higgs boson. Changes are sizable in some cases.

The following differences are easily understood:

- In Refs. [17, 18] the results for $\mathrm{H} \to \mathrm{ZZ}^{(*)} \to 4\ell$ and $\mathrm{H} \to \mathrm{WW}^{(*)} \to \ell\nu\ell\nu$ are evaluated for $m_{\mathrm{H}} = 125.6\,\mathrm{GeV}$, the mass measured in the $\mathrm{H} \to \mathrm{ZZ}^{(*)} \to 4\ell$ analysis. In the present combination the results are evaluated for $m_{\mathrm{H}} = 125.0\,\mathrm{GeV}$, the combined mass measurement from the $\mathrm{H} \to \gamma\gamma$ and $\mathrm{H} \to \mathrm{ZZ}^{(*)} \to 4\ell$ analyses. For values of m_{H} in this region, the branching fractions for $\mathrm{H} \to \mathrm{ZZ}^{(*)} \to 4\ell$ and $\mathrm{H} \to \mathrm{WW}^{(*)} \to \ell\nu\ell\nu$ vary rapidly with m_{H}. For the change of m_{H} in question, $\mathcal{B}(\mathrm{H} \to \mathrm{ZZ}^{(*)} \to 4\ell)$ drops by 5% (relative) and $\mathcal{B}(\mathrm{H} \to \mathrm{WW}^{(*)} \to \ell\nu\ell\nu)$ drops by 4% (relative) [27]. Therefore, when measuring the signal strength relative to the SM expectation, an immediate increase of the same order is expected.
- The $\mathrm{H} \to \tau\tau$ analysis of Ref. [19] focused on exploring the coupling of the tau lepton to the Higgs boson. For this reason nearly all results in Ref. [19] were obtained by treating the $\mathrm{H} \to \mathrm{WW}$ contribution as a background, set to the SM expectation. In the present combination, both the $\mathrm{H} \to \tau\tau$ and $\mathrm{H} \to \mathrm{WW}$ contributions are considered as signal in the $\tau\tau$ decay tag analysis, leading to an increased sensitivity to the presence of a Higgs boson.

4 Results

In this section the results of the combination are presented. We first present a precise measurement of the mass of the new boson using the high-resolution $\mathrm{H} \to \gamma\gamma$ and $\mathrm{H} \to \mathrm{ZZ}^{(*)} \to 4\ell$ channels. Next, we assess the significance of the observed excesses at the best-fit mass value. Finally, we evaluate the consistency of the data observed in the different channels with the expectations for a SM Higgs boson with mass equal to the mass of the observed boson.

4.1 Mass of the observed state

To measure the mass of the observed state, we use the $\mathrm{H} \to \mathrm{ZZ}^{(*)} \to 4\ell$ and $\gamma\gamma$ channels, which have excellent mass resolution. Figure 1 shows 2D 68% CL regions for two parameters of interest, the signal strength relative to the SM expectation, $\mu = \sigma/\sigma_{\mathrm{SM}}$, and the mass, m_{H}, based on these channels. The combined 68% CL confidence region, bounded by a black curve in Fig. 1, is calculated assuming the SM Higgs boson relative event yields between the two channels, while the overall signal strength is left as a free parameter.

To extract the value of m_{H} in a way that is not completely dependent on the SM relative production and decay ratios, the signal strength modifiers for the $(\mathrm{ggH}, \mathrm{t\bar{t}H}) \to \gamma\gamma$, $(\mathrm{VBF}, \mathrm{VH}) \to \gamma\gamma$, and $\mathrm{pp} \to \mathrm{H} \to \mathrm{ZZ}^{(*)} \to 4\ell$ processes are assumed to be independent and therefore not tied to the SM expectation. The signal in all channels is assumed to be due to a single state with mass m_{H}. The best-fit value of m_{H} and its uncertainty are extracted from a scan of the combined test statistic $q(m_{\mathrm{H}})$ with the three signal strength modifiers profiled together with all other nuisance parameters. Figure 2 (left) shows the scan of the test statistic as a function of the mass m_{H} separately for the two channels and for their combination. The intersections of the $q(m_{\mathrm{H}})$ curves with the thick horizontal line at 1.00 and thin line at 3.84 define the 68% and 95% CL intervals for the mass of the observed particle, respectively. These intervals include both the statistical

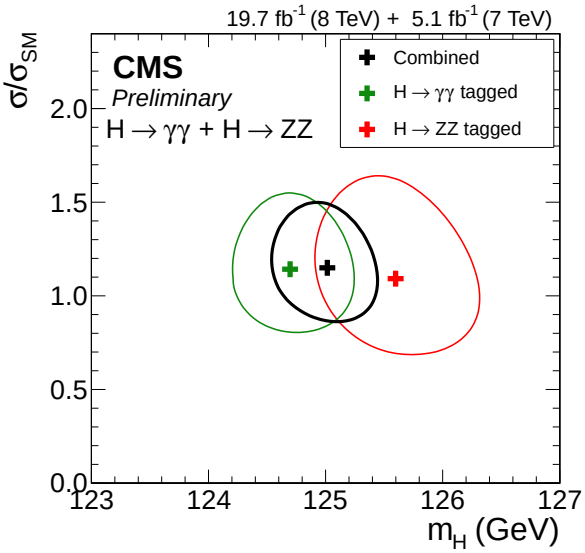

Figure 1: The 68% CL contours for the signal strength $\sigma/\sigma_{\mathrm{SM}}$ versus the boson mass $\mathrm{m_H}$ for the $\gamma\gamma$ (green) and 4ℓ (red) final states, and their combination (black). The symbol $\sigma/\sigma_{\mathrm{SM}}$ denotes the production cross section times the relevant branching fractions, relative to the SM expectation. In this combination, the relative signal strength for the two decay modes is set to the expectation for the SM Higgs boson.

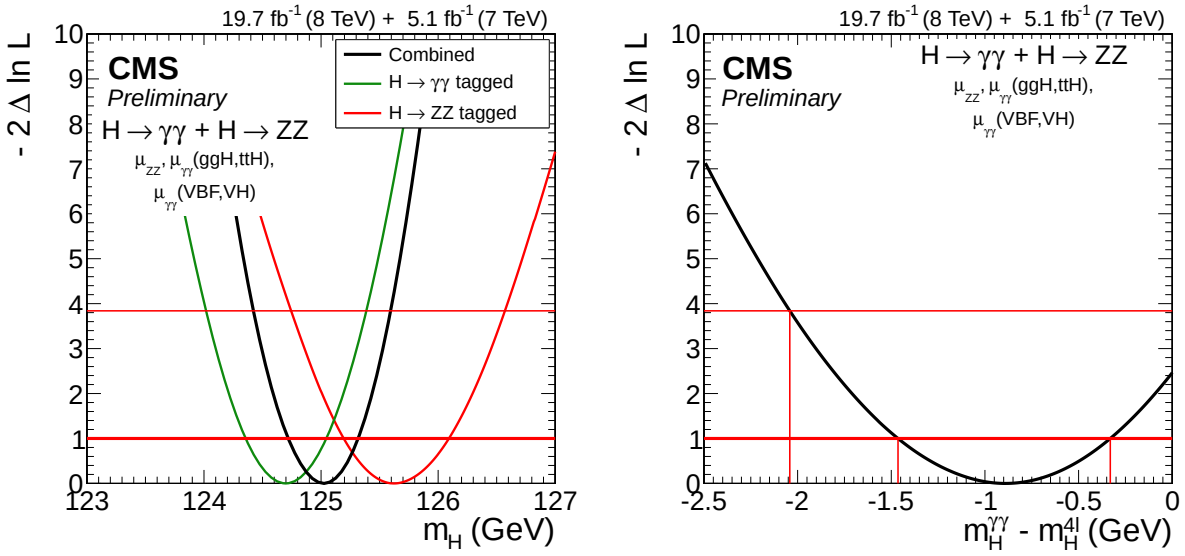

Figure 2: (Left) Scan of the test statistic $q(m_{\mathrm{H}}) = -2\,\Delta \ln \mathcal{L}$ versus the boson mass m_{H} for the $\gamma\gamma$ (green) and 4ℓ (red) final states separately and for their combination (black). Three independent signal strengths, $(\mathrm{ggH}, \mathrm{t\bar{t}H}) \to \gamma\gamma$, $(\mathrm{VBF}, \mathrm{VH}) \to \gamma\gamma$, and $\mathrm{pp} \to \mathrm{H} \to \mathrm{ZZ}^{(*)} \to 4\ell$, are profiled together with all other nuisance parameters. (Right) Scan of the test statistic $q(m_{\mathrm{H}}^{\gamma\gamma} - m_{\mathrm{H}}^{4\ell})$ versus the difference between two individual mass measurements for the same model used in the left panel.

and systematic uncertainties. The mass is measured to be $m_{\mathrm{H}} = 125.03^{+0.29}_{-0.31}$ GeV. To quantify the compatibility of the two individual measurements with each other, we perform a scan of the test statistic $q(m_{\mathrm{H}}^{\gamma\gamma} - m_{\mathrm{H}}^{4\ell})$, as a function of the difference between two mass measurements. There are two degrees of freedom in this test, namely the mass difference and $m_{\mathrm{H}}^{\gamma\gamma}$, which is profiled in the scan. The result is $m_{\mathrm{H}}^{\gamma\gamma} - m_{\mathrm{H}}^{4\ell} = -0.87^{+0.54}_{-0.59}$ GeV and is shown in Fig. 2 (right); the two measurements agree at the 1.6σ level.

To evaluate the statistical component of the overall uncertainty, we also perform a scan of $q(m_{\mathrm{H}})$ fixing all nuisance parameters to their best-fit values, except for those related to the $\mathrm{H} \to \gamma\gamma$ background models; given how the $\mathrm{H} \to \gamma\gamma$ background distributions are modeled from fits to data, their degrees of freedom encode fluctuations which are statistical in nature. The result is shown by the dashed curve in Fig. 3. The crossings of the dashed curve with the thick horizontal line define the 68% CL interval for the statistical uncertainty in the mass measurement: $^{+0.26}_{-0.27}$ GeV. We derive the systematic uncertainty assuming that the total uncertainty is the sum in quadrature of the statistical and systematic components; the full result can be written as $m_{\mathrm{H}} = 125.03\,^{+0.26}_{-0.27}\,(\mathrm{stat.})\,^{+0.13}_{-0.15}\,(\mathrm{syst.})\,\mathrm{GeV}$. The expected uncertainty is evaluated using an Asimov pseudo-data set [34] constructed from the best-fit values obtained when testing for the compatibility of the mass measurement in the $\mathrm{H} \to \gamma\gamma$ and $\mathrm{H} \to \mathrm{ZZ}^{(*)} \to 4\ell$ channels. The expected uncertainty thus derived is $^{+0.26}_{-0.25}\,(\mathrm{stat.}) \pm 0.14\,(\mathrm{syst.})\,\mathrm{GeV}$, in good agreement with the observation in data. As a comparison, the expected uncertainty is also derived by constructing an Asimov pseudo-data set as above except that the signal strength modifiers are set to unity (as expected in the SM), $m_{\mathrm{H}}^{\gamma\gamma} = 125\,\mathrm{GeV}$, and $m_{\mathrm{H}}^{\gamma\gamma} - m_{\mathrm{H}}^{4\ell} = 0\,\mathrm{GeV}$, leading to $\pm 0.28\,(\mathrm{stat.}) \pm 0.13\,(\mathrm{syst.})\,\mathrm{GeV}$. As could be anticipated, the statistical uncertainty is slightly larger given that the observed signal strength in the $\mathrm{H} \to \gamma\gamma$ channel is larger than unity, and the systematic uncertainty is slightly smaller given the small observed mass difference between the two channels.

To assess the dependency of the mass measurement on the SM Higgs boson hypothesis, the measurement is repeated using the same channels, but with the following two sets of assumptions: i) allowing a common signal strength modifier to float, which corresponds to the result in Fig. 1, and ii) constraining the relative production cross sections and branching fractions to the SM predictions, i.e., $\mu = 1$. The results from these two alternative measurements differ by less than 0.1 GeV with respect to the main result, both in terms of the best-fit value and the uncertainties.

4.2 Significance of the observed excess

Table 2 summarizes the median expected and observed local significance for a SM Higgs boson mass of 125.0 GeV from the different decay mode tags, grouped as described in Section 3.3. The value of m_{H} is fixed to the best-fit combined measurement presented in Section 4.1. The expected significance values are evaluated using the post-fit expected background rates and the signal rates expected from the SM. The $\pm 1\sigma$ range around the median significance contains approximately 68% of the statistical fluctuations that could occur in data, except for the ZZ channel; given the high signal-to-background ratio in the ZZ channel, 68% of the statistical fluctuations that could occur in data are contained in a range of $\pm 1.4\sigma$ around the median expected significance.

In each decay group the probability is low for a statistical fluctuation of the background to produce an excess at least as large as that observed. Differences between the results Table 2 and the individual publications are understood in terms of the discussion in Sections 3.3 and 3.4, namely the grouping of channels by decay mode tag, the change of m_{H} for which the

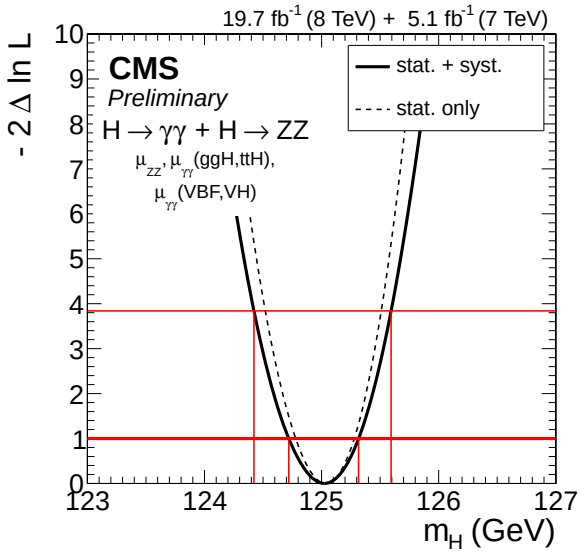

Figure 3: Scans of the test statistic $q(m_{\mathrm{H}})$ versus the boson mass m_{H} for the combination of the $\gamma\gamma$ and 4ℓ analyses. The solid curve is obtained by profiling all nuisance parameters and thus includes both statistical and systematic uncertainties, as in Fig. 2 (left). The dashed curve is obtained by fixing all nuisance parameters to their best-fit values, except for those related to the $\mathrm{H} \to \gamma\gamma$ background description, thus including only statistical uncertainties. The crossings with the thick (thin) horizontal lines define the 68% (95%) CL interval for the measured mass.

Table 2: The median observed and expected significances of the excesses for $m_{\mathrm{H}} = 125.0\,\mathrm{GeV}$ of the combinations of decay mode groups. The channels are grouped by decay mode tag as described in Section 3.3; when there is a difference in the channels included with respect to the published results for the individual channels, the result for the grouping used in those publications is also given.

Channel grouping	Significance (σ)	
	Observed	Expected
$\mathrm{H} \to \mathrm{ZZ}$ tagged	6.5	6.3
$\mathrm{H} \to \gamma\gamma$ tagged	5.6	5.3
$\mathrm{H} \to \mathrm{WW}$ tagged	4.7	5.4
Grouped as in Ref. [17]	*4.3*	*5.4*
$\mathrm{H} \to \tau\tau$ tagged	3.8	3.9
Grouped as in Ref. [19]	*3.9*	*3.9*
$\mathrm{H} \to \mathrm{bb}$ tagged	2.0	2.3
Grouped as in Ref. [16]	*2.1*	*2.3*

significance of the $H \to ZZ^{(*)} \to 4\ell$ and $H \to WW^{(*)} \to \ell\nu\ell\nu$ analyses is evaluated, and the treatment of $H \to WW$ as part of the signal, instead of background, in the $H \to \tau\tau$ analysis.

Finally, the $\gamma\gamma$ and $H \to ZZ^{(*)} \to 4\ell$ decay modes indicate that the new particle is a boson, and the diphoton decay implies that its spin is different from unity [38, 39]. The observed data have been shown to disfavor spin-2 hypotheses and, assuming that the boson has zero spin, to be consistent with the pure scalar hypothesis, while disfavoring the pure pseudoscalar hypothesis [17, 18].

4.3 Compatibility of the observed state with the SM Higgs boson hypothesis

The size of the current data set allows only a limited number of compatibility tests of the observed excesses with the expected SM signal. These tests are presented in this subsection. These compatibility tests do not constitute measurements of any physics parameters per se, but rather probe the consistency of the various observations with the expectations for the SM Higgs boson.

4.3.1 Signal strength in combination and subcombinations

The best-fit value for the common signal strength modifier $\hat{\mu} = \hat{\sigma}/\sigma_{\mathrm{SM}}$, obtained in the combination of all search channels, provides the first compatibility test. In the formal fit, $\hat{\mu}$ is allowed to become negative if the observed number of events is smaller than the expected yield for the background-only hypothesis. The observed $\hat{\mu}$ value for a Higgs boson mass $m_{\mathrm{H}} = 125.0\,\mathrm{GeV}$ is 1.00 ± 0.13, consistent with unity, as expected for the SM Higgs boson by construction. The uncertainty can be further broken down into a statistical component (stat.), a component associated with QCD scale variations, parton distribution functions, branching fractions, underlying event description (theo.), and any other systematic uncertainties (syst.); the result is $1.00 \pm 0.09\,(\mathrm{stat.})\,^{+0.08}_{-0.07}\,(\mathrm{theo.}) \pm 0.07\,(\mathrm{syst.})$.

Figure 4 shows the $\hat{\mu}$ values obtained in different subcombinations of channels for $m_{\mathrm{H}} = 125.0\,\mathrm{GeV}$, grouped by predominant decay mode or by additional tags targeting events from particular production mechanisms. As discussed in Section 3.3 the expected purities of the different tagged samples vary substantially. Therefore, these plots cannot be interpreted literally as compatibility tests for pure production mechanisms or decay modes. The mix of production and decay modes is naturally handled in terms of deviations in the magnitudes of the SM Higgs boson scalar couplings, presented in Section 4.3.2.

The level of compatibility of any subcombination with the SM Higgs boson cross section can be quantified by the value of the test statistic

$$q_\mu = -2\,\Delta \ln \mathcal{L} = -2 \ln \frac{\mathcal{L}(\mathrm{data} \,|\, \mu, \hat{\theta}_\mu)}{\mathcal{L}(\mathrm{data} \,|\, \hat{\mu}, \hat{\theta})} \tag{5}$$

at $\mu = 1$, which, asymptotically in the limit of large statistics, has a χ^2 distribution. For N subcombinations, the sum of the individual $q_\mu(\mu = 1)$ values is expected to behave asymptotically as a χ^2 distribution with N degrees of freedom (dof).

The sixteen subchannel combination shown in Fig. 4 (top) gives a $\chi^2/(\mathrm{dof}) = 10.5/16$, which corresponds to an asymptotic p-value of 0.84. The five subcombinations by decay mode tag shown in Fig. 4 (bottom left) yield a $\chi^2/(\mathrm{dof}) = 0.9/5$ and an asymptotic p-value of 0.97. Figure 4 (bottom right) shows an excess in the $\mathrm{t\bar{t}H}$-tagged subcombination, due to the observations in the $\mathrm{t\bar{t}H}$-tagged $H \to \gamma\gamma$ and $H \to$ leptons analyses that can be seen in the top panel. The sub-

Table 3: The best-fit values for the signal strength at $m_{\mathrm{H}} = 125.0\,\mathrm{GeV}$, of the VBF and VH, and of the ggH and $\mathrm{t\bar{t}H}$ production mechanisms, $\mu_{\mathrm{VBF,VH}}$ and $\mu_{\mathrm{ggH,t\bar{t}H}}$, respectively. The channels are grouped by decay mode tag as described in Section 3.3. The observed and median expected results for the ratio of $\mu_{\mathrm{VBF,VH}}$ to $\mu_{\mathrm{ggH,t\bar{t}H}}$ together with their uncertainties are also given for the full combination.

Channel grouping	Best fit $(\mu_{\mathrm{ggH,t\bar{t}H}}, \mu_{\mathrm{VBF,VH}})$
$\mathrm{H} \to \mathrm{ZZ}$ tagged	$(0.88, 1.75)$
$\mathrm{H} \to \gamma\gamma$ tagged	$(1.07, 1.24)$
$\mathrm{H} \to \mathrm{WW}$ tagged	$(0.87, 0.66)$
$\mathrm{H} \to \tau\tau$ tagged	$(0.52, 1.21)$
$\mathrm{H} \to \mathrm{bb}$ tagged	$(0.57, 0.96)$
Combined best fit $\mu_{\mathrm{VBF,VH}}/\mu_{\mathrm{ggH,t\bar{t}H}}$	
	Observed (expected)
	$1.25^{+0.63}_{-0.45}$ $(1.00^{+0.49}_{-0.35})$

combinations by production process tag have a $\chi^2/(\mathrm{dof}) = 5.3/4$ and an asymptotic p-value of 0.26, clearly driven by the excess observed in the analyses tagging the $\mathrm{t\bar{t}H}$ production process.

The p-values above indicate that the extracted signal strengths in these subcombinations are compatible with the SM prediction for the Higgs boson, $\mu = 1$. The result of the $\mathrm{t\bar{t}H}$-tagged subcombination is compatible with the SM hypothesis at the 2.0σ level.

The four main Higgs boson production mechanisms can be associated with either fermion couplings (ggH and $\mathrm{t\bar{t}H}$) or vector-boson couplings (VBF and VH) of the Higgs boson. Therefore, a combination of channels associated with a particular decay mode tag, but explicitly targeting different production mechanisms, can be used to test the relative strengths of the couplings to the vector bosons and fermions (mainly the top quark). The categorization of the different channels into production mode tags is not pure and contributions from the different signal processes are evaluated from Monte Carlo simulation and taken into account in the fits. Figure 5 (left) shows the 68% CL confidence regions for the signal strength modifiers associated with the ggH and $\mathrm{t\bar{t}H}$, and with the VBF and VH production mechanisms, $\mu_{\mathrm{ggH,t\bar{t}H}}$ and $\mu_{\mathrm{VBF,VH}}$, respectively. The five sets of contours correspond to the five combinations by predominant decay mode as presented in Table 2. The SM Higgs boson expectation of $(1, 1)$ is within the 68% CL regions in all cases. The best-fit values for each decay mode group are given in Table 3.

The ratio of $\mu_{\mathrm{VBF,VH}}$ and $\mu_{\mathrm{ggH,t\bar{t}H}}$ can also be measured in each decay mode group. In this ratio the branching fractions cancel out in each channel and the results of the different channels can be combined. Figure 5 (right) shows the corresponding likelihood scan of the data for this ratio.

Figure 6 shows the results of scans of four independent signal strengths corresponding to the four SM main production processes, assuming the relative branching fractions of the SM; the best-fit results are given in Table 4. From the scan on the top left, the μ_{ggH} best-fit value is found to be $0.85^{+0.19}_{-0.17}$. After calculating the component of the uncertainty that is statistical in nature (stat.) and that which is related to the theory inputs (theo.), one can then subtract them in quadrature from the total uncertainty and assign the remainder as systematic uncertainty (syst.), yielding $0.85\,^{+0.11}_{-0.09}$ (stat.) $^{+0.11}_{-0.08}$ (theo.) $^{+0.10}_{-0.09}$ (syst.).

It is also interesting to probe the vector-boson production mechanisms and assess independently the signal strengths for the VH and VBF modes. Likelihood scans are performed versus

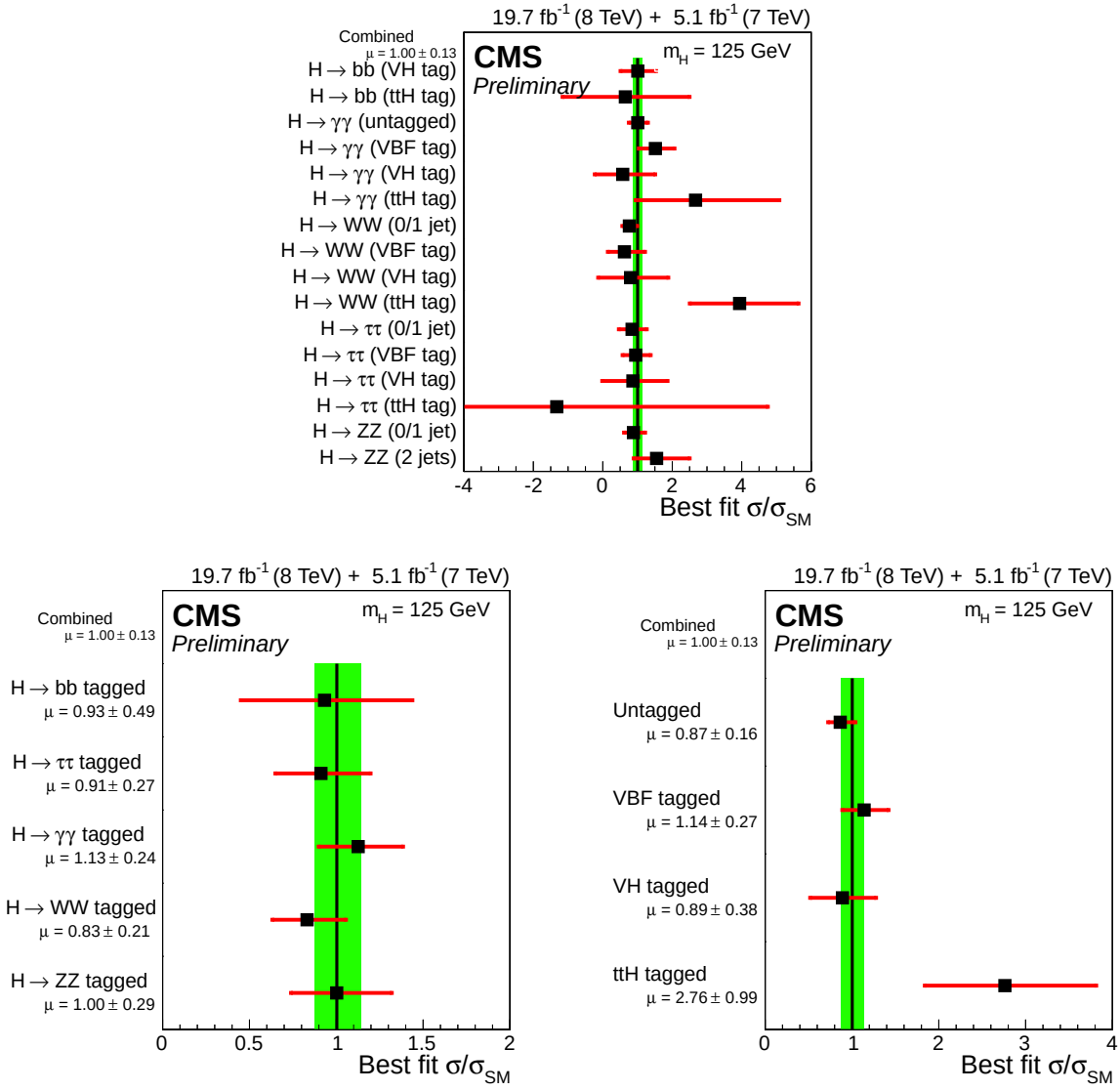

Figure 4: Values of the best-fit $\sigma/\sigma_{\mathrm{SM}}$ for the combination (solid vertical line), for individual channels, and for subcombinations by predominant decay mode or production mode tag. The vertical band shows the overall $\sigma/\sigma_{\mathrm{SM}}$ uncertainty. The $\sigma/\sigma_{\mathrm{SM}}$ ratio denotes the production cross section times the relevant branching fractions, relative to the SM expectation. The horizontal bars indicate the ± 1 standard deviation uncertainties in the best-fit $\sigma/\sigma_{\mathrm{SM}}$ values for the individual modes; they include both statistical and systematic uncertainties. (Top) Subcombinations by predominant decay mode and additional tags targeting a particular production mechanism. (Bottom left) Subcombinations by predominant decay mode. (Bottom right) Subcombinations by analysis tags targeting individual production mechanisms; the excess in the $\mathrm{t\bar{t}H}$-tagged subcombination is largely driven by the $\mathrm{t\bar{t}H}$-tagged $\mathrm{H} \to \gamma\gamma$ and $\mathrm{H} \to \mathrm{WW}$ channels as can be seen in the top panel.

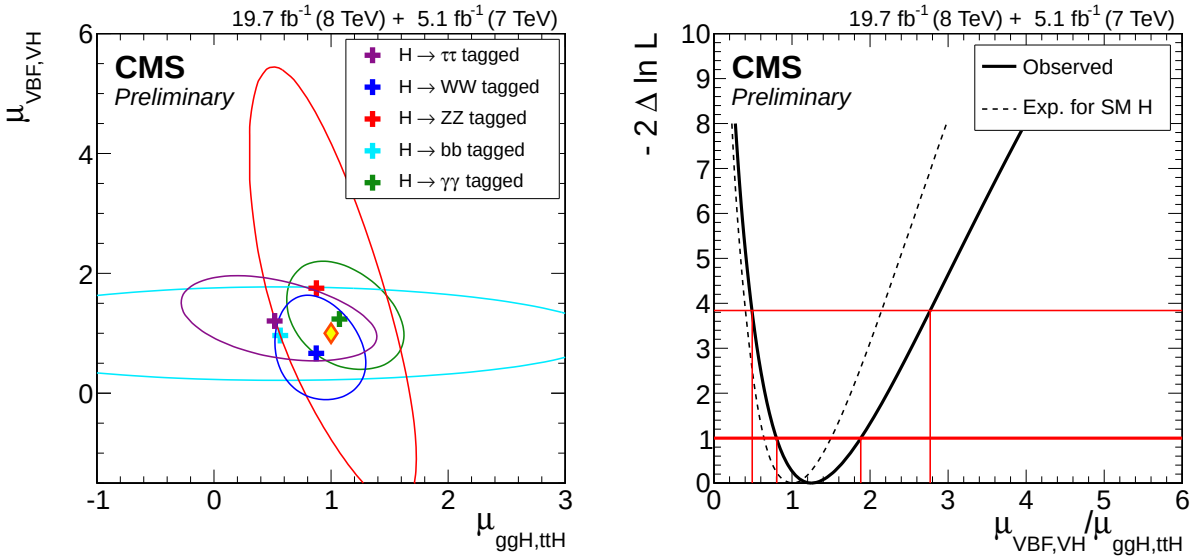

Figure 5: (Left) The 68% CL regions (bounded by the solid curves) for the signal strength of the ggH and $t\bar{t}H$, and of the VBF and VH production mechanisms, $\mu_{ggH,t\bar{t}H}$ and $\mu_{VBF,VH}$, respectively. The different colors show the results obtained by combining data from each group of predominant decay modes: $\gamma\gamma$ (green), WW (blue), ZZ (red), $\tau\tau$ (violet), bb (cyan). The crosses indicate the best-fit values. The diamond at $(1,1)$ indicates the expected values for the SM Higgs boson. (Right) Likelihood scan versus the ratio of $\mu_{VBF,VH}/\mu_{ggH,t\bar{t}H}$ combined for all channels. The solid curve represents the observed result in data while the dashed curve indicates the expected median result in the presence of the SM Higgs boson. Crossings with the horizontal thick and thin red lines denote the 68% CL and 95% CL confidence intervals.

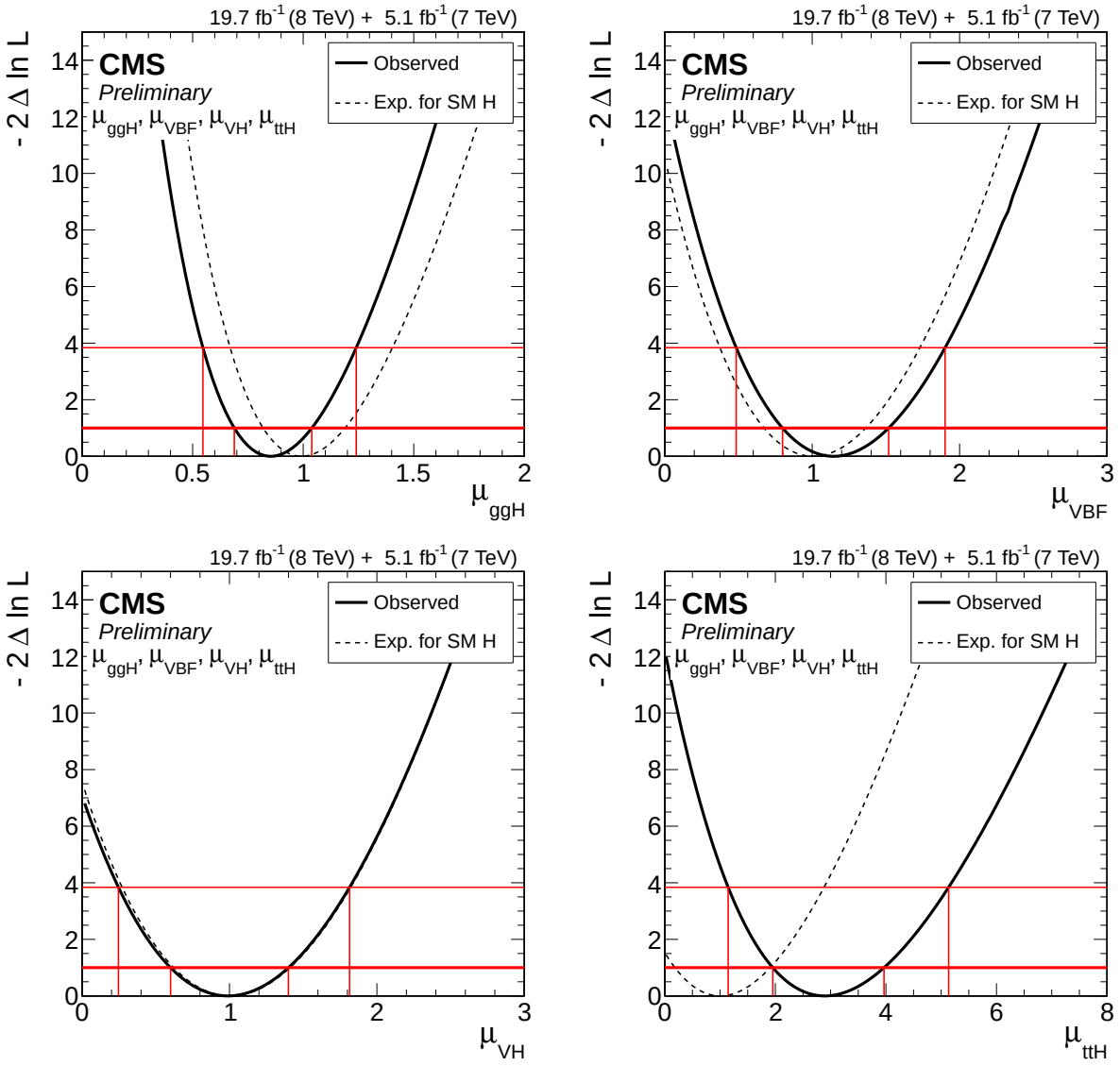

Figure 6: Likelihood scan versus μ_{ggH} (top left), μ_{VBF} (top right), μ_{VH} (bottom left), and $\mu_{\mathrm{t\bar{t}H}}$ (bottom right). The solid curve is the result observed in data. The dashed curve indicates the expected median results in the presence of the SM Higgs boson. Crossings with the horizontal thick and thin red lines denote the 68% CL and 95% CL confidence intervals.

μ_{VBF} and μ_{VH} respectively, allowing the modifiers associated with the three other production processes to float in the fit together with the nuisance parameters. All the decay mode groups are used for this test, with the results mainly driven by the corresponding tagged categories, while the contribution from ggH is constrained by the 0-jet and untagged categories. The plots in Fig. 6 display the results of the scans, on the top right for VBF and on the bottom left for VH. The median expected results for the SM Higgs boson are represented by the dashed curves, in good agreement with the results from the data (solid curves).

Finally, the large best-fit value for $\mu_{\mathrm{t\bar{t}H}}$ is compatible with what was seen and discussed in Fig. 4; the data are compatible with the $\mu_{\mathrm{t\bar{t}H}} = 1$ hypothesis at the 2.1σ level.

Table 4: The best-fit results for independent signal strengths corresponding to the four main production processes, ggH, VBF, VH, and $\mathrm{t\bar{t}H}$. These results assume the relative values of the branching fractions to be those of the SM.

Parameter	Best-fit result (68% CL)
μ_{ggH}	$0.85^{+0.19}_{-0.17}$
μ_{VBF}	$1.15^{+0.37}_{-0.35}$
μ_{VH}	$1.00^{+0.40}_{-0.40}$
$\mu_{\mathrm{t\bar{t}H}}$	$2.93^{+1.04}_{-0.97}$

4.3.2 Compatibility of the observed data with the SM Higgs boson couplings

Following the framework laid out in Ref. [27], the event yield in a given (production)$\times$(decay) mode is assumed to be related to the production cross section and the partial and total Higgs boson decay widths via the following equation:

$$(\sigma \cdot \mathcal{B})\,(x \to \mathrm{H} \to ff) = \frac{\sigma_x \cdot \Gamma_{ff}}{\Gamma_{\mathrm{tot}}}, \tag{6}$$

where σ_x is the production cross section through the initial state x (x includes ggH, VBF, WH and ZH, and $\mathrm{t\bar{t}H}$); Γ_{ff} is the partial decay width into the final state ff, such as WW, ZZ, bb, $\tau\tau$, or $\gamma\gamma$; and Γ_{tot} is the total width of the Higgs boson.

In particular, σ_{ggH}, Γ_{gg}, and $\Gamma_{\gamma\gamma}$ are generated by loop diagrams and are directly sensitive to the presence of new physics. The possibility of Higgs boson decays to particles beyond the standard model (BSM), with a partial width Γ_{BSM}, is accommodated by keeping Γ_{tot} as a dependent parameter so that $\Gamma_{\mathrm{tot}} = \sum \Gamma_{ff} + \Gamma_{\mathrm{BSM}}$, where the $\sum \Gamma_{ff}$ stands for the sum over partial widths for all accessible decays to pairs of SM particles. The partial widths are proportional to the squares of the effective Higgs boson couplings to the corresponding particles. To test for possible deviations in the data from the rates expected in the different channels for the SM Higgs boson, we introduce coupling modifiers, denoted by scale factors κ_i, and fit for these parameters [27]. Here i can stand for V (vector bosons), W (W boson), Z (Z boson), f (fermions), ℓ (leptons), q (quarks), u (up-type leptons and quarks), d (down-type leptons and quarks), b (b quarks), t (top quark), τ (tau lepton), g (gluon, i.e., not resolving the loop), γ (photon, i.e., not resolving the loop). Significant deviations of any κ from unity would imply new physics beyond the SM Higgs boson hypothesis.

The size of the current data set is insufficient to fully quantify all eight phenomenological parameters defining the Higgs boson production and decay rates. Therefore, we present a range of combinations with fewer degrees of freedom where the remaining unmeasured degrees of freedom are either constrained to be equal to the SM Higgs boson expectations or profiled in the likelihood scans together with all other nuisance parameters.

The mass is fixed to the measured value of 125.0 GeV. Since results for the individual channels are based on different assumed values of the mass, differences should be expected when comparing the results from the individual channels and those in this combination.

Test of custodial symmetry In the SM, the Higgs sector possesses a global $\mathrm{SU(2)_L \times SU(2)_R}$ symmetry, which is broken by the Higgs vacuum expectation value down to the diagonal subgroup $\mathrm{SU(2)_{L+R}}$. As a result, the tree-level ratios between the W and Z boson masses, $m_{\mathrm{W}}/m_{\mathrm{Z}}$, and their couplings to the Higgs boson, $g_{\mathrm{W}}/g_{\mathrm{Z}}$, are protected against large radiative correc-

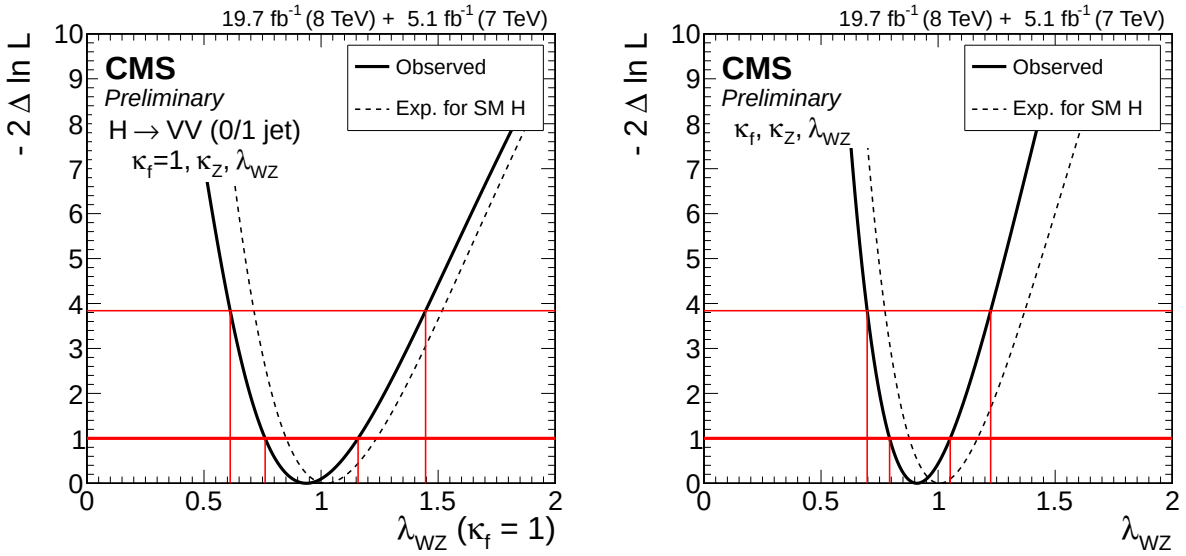

Figure 7: Likelihood scans versus λ_{WZ}, the ratio of the couplings to W and Z bosons: (left) from untagged $pp \to H \to WW$ and $pp \to H \to ZZ$ searches, assuming SM couplings to fermions, $\kappa_f = 1$; (right) from the combination of all channels, profiling the coupling to fermions. The solid curve represents the observation in data. The dashed curve indicates the expected median results in the presence of the SM Higgs boson. Crossings with the horizontal thick and thin red lines denote the 68% CL and 95% CL confidence intervals.

tions, a property known as "custodial symmetry" [40, 41]. However, large violations of custodial symmetry are possible in new physics models. To test the custodial symmetry, we introduce two scaling factors κ_W and κ_Z that modify the SM Higgs boson couplings to the W and Z bosons and perform two combinations to assess the consistency of the ratio $\lambda_{WZ} = \kappa_W/\kappa_Z$ with unity.

The dominant production mechanism populating the untagged channels of the $H \to WW^{(*)} \to \ell\nu\ell\nu$ and $H \to ZZ^{(*)} \to 4\ell$ analyses is ggH. Therefore, the ratio of event yields in these channels provides a nearly model-independent measurement of λ_{WZ}. We perform a combination of these two channels with two free parameters, κ_Z and λ_{WZ}. The likelihood scan versus λ_{WZ} is shown in Fig. 7 (left). The scale factor κ_Z is treated as a nuisance parameter. The result is $\lambda_{WZ} = 0.94^{+0.22}_{-0.18}$, i.e., the data are consistent with the SM expectation ($\lambda_{WZ} = 1$).

We also extract λ_{WZ} from the overall combination of all channels. In this approach, we introduce three degrees of freedom: λ_{WZ}, κ_Z, and κ_f. The BSM Higgs boson width Γ_{BSM} is set to zero. The partial width Γ_{gg}, induced by the quark loops, scales as κ_f^2. The partial width $\Gamma_{\gamma\gamma}$ is induced via loop diagrams, with the W boson and top quark being the dominant contributors, and is scaled according to Eq. 113 of Ref. [27]. In the likelihood scan $q(\lambda_{WZ})$, both κ_Z and κ_f are profiled together with all other nuisance parameters. The introduction of one common scaling factor for all fermions makes this measurement model-dependent, but using all channels gives it greater statistical power. The likelihood scan is shown in Fig. 7 (right) with a solid curve. The dashed curve indicates the median expected result for the SM Higgs boson, given the current data set. The measured value from the combination of all channels is $\lambda_{WZ} = 0.91^{+0.14}_{-0.12}$ and is consistent with the expectation set by custodial symmetry.

Unless otherwise noted, in all further combinations we assume $\lambda_{WZ} = 1$ and use a common factor κ_V to modify the couplings to W and Z bosons, whilst preserving their ratio.

Test of the couplings to vector bosons and fermions We compare the observation with the expectation for the standard model Higgs boson by fitting two parameters, κ_V and κ_f, as previously defined. We assume that $\Gamma_{BSM} = 0$. At leading order (LO), all partial widths, except for $\Gamma_{\gamma\gamma}$, scale either as κ_V^2 or κ_f^2. As discussed above, the partial width $\Gamma_{\gamma\gamma}$ is induced via loops of virtual W bosons or top quarks and scales as a function of κ_V and κ_f. For that reason, the $\gamma\gamma$ channel is the only channel that is sensitive to the relative sign of κ_V and κ_f.

Figure 8 shows the 2D likelihood scan over the (κ_V, κ_f) phase space. The left plot allows for different signs of κ_V and κ_f, while the right plot constrains the phase space to the $(+,+)$ quadrant. The 68%, 95%, and 99.7% CL confidence regions for κ_V and κ_f are shown with solid, dashed, and dotted curves, respectively. The data are compatible with the expectation for the standard model Higgs boson: the point $(\kappa_V, \kappa_f) = (1,1)$ is within the 68% confidence region defined by the data. By the nature of the way these compatibility tests are constructed, any significant deviations from $(1,1)$, should they be observed, would not have straightforward interpretations within the SM and would imply BSM physics; the scale/sign of the best-fit values in such an eventuality would guide us toward identifying the most plausible BSM scenarios. Figure 9 shows the interplay of different decay mode groups. The 95% CL intervals for κ_V and κ_f are each obtained from a 1D scan where the other parameter is fixed to unity, and equal [0.88,1.15] and [0.64,1.16], respectively.

Test for the presence of BSM particles The presence of BSM physics can considerably modify the Higgs boson phenomenology even if the underlying Higgs boson sector in the model remains unaltered. Processes induced by loop diagrams ($H \to \gamma\gamma$ and ggH) can be particularly susceptible to the presence of new particles. Therefore, we combine and fit the data for the scale factors (κ_γ and κ_g) for these two processes. The partial widths associated with the tree-level production processes and decay modes are assumed to be unaltered.

Figure 10 shows the 2D likelihood scan for the κ_g and κ_γ parameters (assuming $\Gamma_{BSM} = 0$). The results are compatible with the expectation for the SM Higgs boson as the point $(\kappa_\gamma, \kappa_g) = (1,1)$ is within the 95% CL region defined by the data. The best-fit point is $(\kappa_\gamma, \kappa_g) = (1.14, 0.88)$, while the 95% CL intervals for each of these scaling factors separately are [0.89,1.42] for κ_γ and [0.69,1.10] for κ_g.

Figure 11 shows the likelihood scan versus $BR_{BSM} = \Gamma_{BSM}/\Gamma_{tot}$, with κ_g and κ_γ profiled together with all other nuisance parameters. The data allow us to conclude that BR_{BSM} is in the interval [0.00,0.32] at 95% CL.

Test for asymmetries in the couplings to fermions In models with two Higgs doublets (2HDM), the couplings of the neutral Higgs bosons to fermions can be substantially modified with respect to the couplings of the SM Higgs boson. For example, in the MSSM, the couplings of neutral Higgs bosons to up-type and down-type fermions are modified, with the modification being the same for all three generations and for quarks and leptons. In more general 2HDMs, leptons can be made to virtually decouple from a Higgs boson that otherwise behaves in a SM-like way with respect to W/Z-bosons and quarks. Inspired by the possibility of such modifications to the fermion couplings, we perform two combinations in which we allow for different ratios of the couplings to down/up fermions ($\lambda_{du} = \kappa_d/\kappa_u$) or different ratios of the couplings to leptons and quarks ($\lambda_{\ell q} = \kappa_\ell/\kappa_q$). We assume that $\Gamma_{BSM} = 0$.

Figure 12 (left) shows the likelihood scan versus λ_{du}, with κ_V and κ_u profiled together with all other nuisance parameters. Figure 12 (right) shows the likelihood scan versus $\lambda_{\ell q}$, with κ_V and κ_q profiled. Both λ_{du} and $\lambda_{\ell q}$ are constrained to be positive; the 95% CL intervals for them are [0.66,1.43] and [0.61,1.49] respectively.

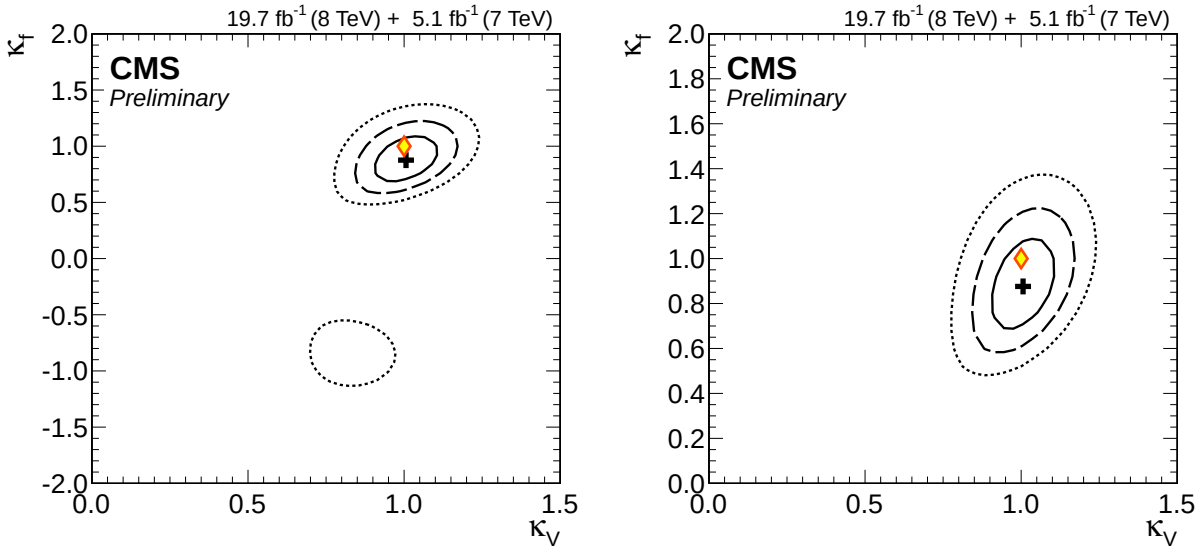

Figure 8: Results of 2D likelihood scans for the κ_V and κ_f parameters. The cross indicates the best-fit values. The solid, dashed, and dotted contours show the 68%, 95%, and 99.7% CL regions, respectively. The yellow diamond shows the SM point $(\kappa_V, \kappa_f) = (1, 1)$. The left plot shows the likelihood scan in two quadrants, $(+,+)$ and $(+,-)$. The right plot shows the likelihood scan constrained to the $(+,+)$ quadrant.

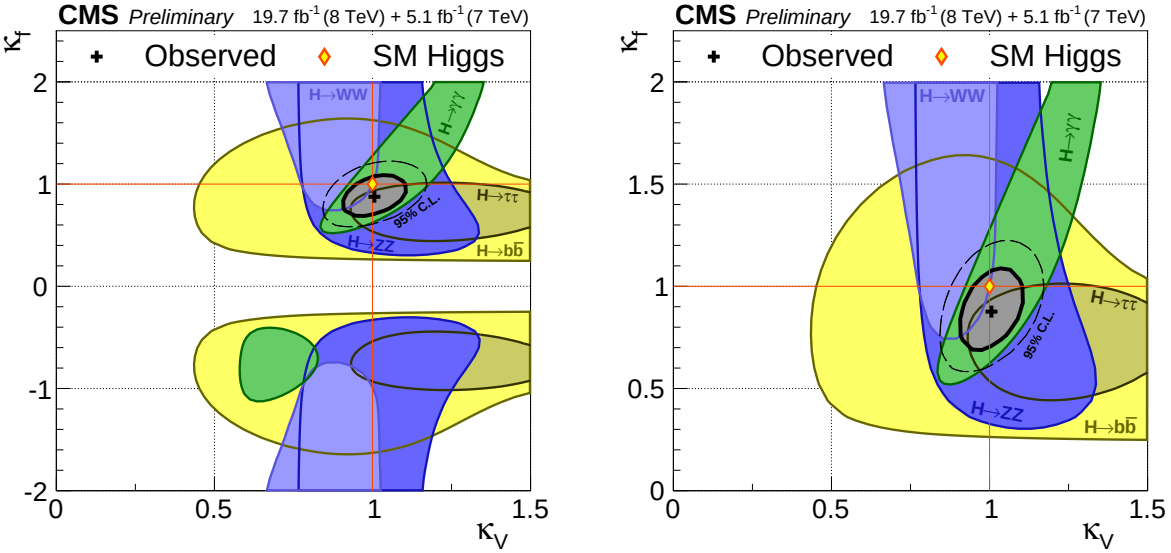

Figure 9: The 68% CL contours for individual channels (colored swaths) and for the overall combination (thick curve) for the (κ_V, κ_f) parameters. The cross indicates the global best-fit values. The dashed contour bounds the 95% CL confidence region for the combination. The yellow diamond represents the SM expectation, $(\kappa_V, \kappa_f) = (1, 1)$. The left plot shows the likelihood scan in two quadrants $(+,+)$ and $(+,-)$, the right plot shows the positive quadrant only.

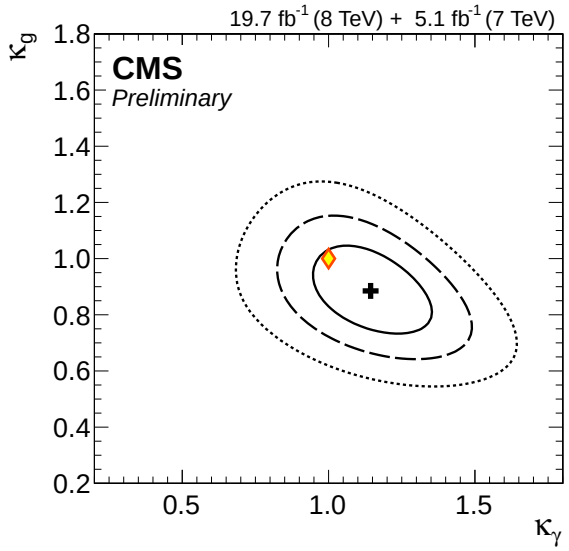

Figure 10: The 2D likelihood scan for the κ_g and κ_γ parameters, assuming that $\Gamma_{BSM} = 0$. The cross indicates the best-fit values. The solid, dashed, and dotted contours show the 68%, 95%, and 99.7% CL regions, respectively. The yellow diamond represents the SM expectation, $(\kappa_\gamma, \kappa_g) = (1, 1)$. The partial widths associated with the tree-level production processes and decay modes are assumed to be unaltered ($\kappa = 1$).

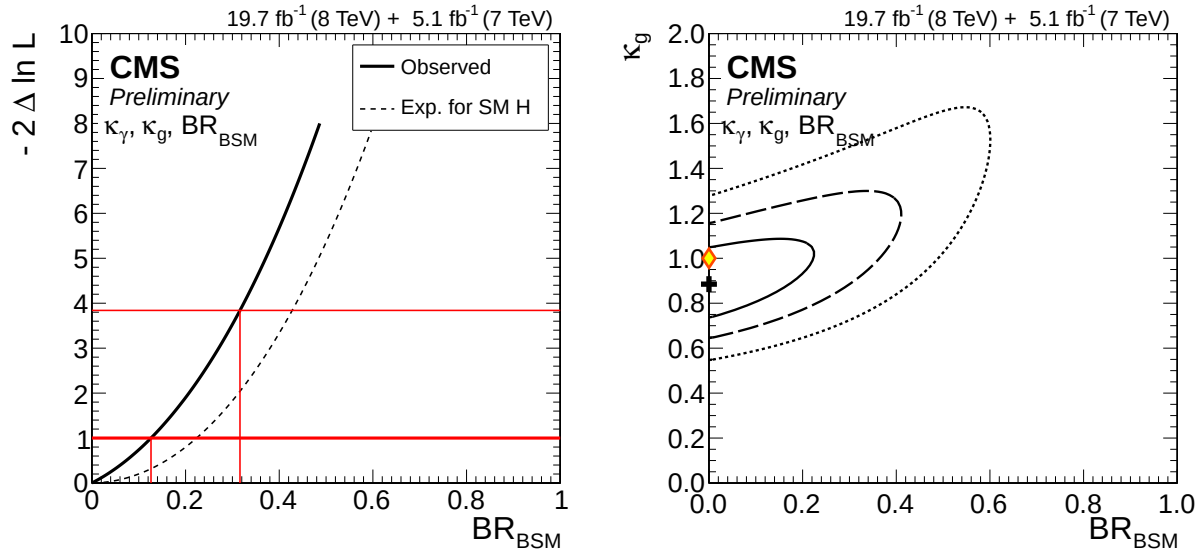

Figure 11: (Left) The likelihood scan versus $BR_{BSM} = \Gamma_{BSM}/\Gamma_{tot}$. The solid curve represents the observation and the dashed curve indicates the expected median results in the presence of the SM Higgs boson. The partial widths associated with the tree-level production processes and decay modes are assumed to be unaltered ($\kappa = 1$). (Right) Correlation between κ_g and BR_{BSM}. The solid, dashed, and dotted contours show the 68%, 95%, and 99.7% CL regions, respectively.

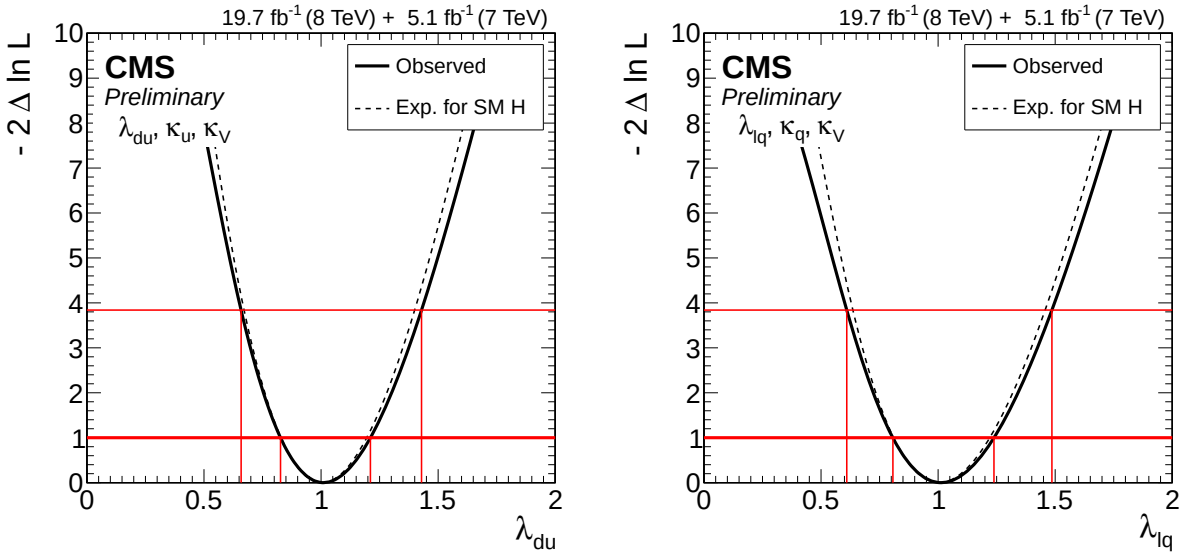

Figure 12: (Left) Likelihood scan versus ratio of couplings to down/up fermions, λ_{du}, with the two other free coupling modifiers, κ_{V} and κ_{u}, profiled together with all other nuisance parameters. (Right) Likelihood scan versus ratio of couplings to leptons and quarks, $\lambda_{\ell\mathrm{q}}$, with the two other free coupling modifiers, κ_{V} and κ_{q}, profiled together with all other nuisance parameters.

Test of a model with six independent scaling factors We explore a model with six independent coupling scaling factors by making the following assumptions:

- The couplings to W and Z bosons are scaled by a common factor κ_V;
- The couplings to third generation fermions, i.e., the top quark, bottom quark, and tau lepton, are scaled independently by κ_t, κ_b, and κ_τ;
- The scale factors for couplings to the first and second generation fermions are equal to those for the third;
- The effective couplings to gluons and photons, induced by loop diagrams, are given independent scaling factors κ_g and κ_γ, respectively;
- The partial width Γ_{BSM} is zero.

The results of the likelihood scans for these six parameters, one at a time while profiling the remaining five together with all other nuisance parameters, are shown in Fig. 13. The current data do not show any statistically significant deviations with respect to the SM Higgs boson hypothesis. For every κ, the measured 95% CL interval contains unity. A goodness-of-fit test between the parameters measured in this model and the SM prediction yields a $\chi^2/(\text{dof}) = 7.5/6$, which corresponds to an asymptotic p-value of 0.28.

Constraints on BR_{BSM} in a scenario with free couplings An alternative, more general scenario than that with six parameters can be obtained by allowing for a non-vanishing Γ_{BSM}, but constraining $\kappa_V \leq 1$, a requirement motivated by electroweak symmetry breaking.

Figure 14 shows the likelihood scan versus BR_{BSM} derived in this scenario while profiling all the other coupling modifiers and nuisance parameters. Within these assumptions, the data allow us to conclude that BR_{BSM} is in the interval [0.00,0.58] at 95% CL.

Summary of tests of the compatibility of the data with the SM Higgs boson couplings Table 5 summarizes the tests performed on the compatibility of the data with the expected SM Higgs boson couplings. No statistically significant deviations are observed.

5 Conclusions

Properties of the Higgs boson with mass near 125 GeV are measured in proton-proton collisions with the CMS experiment at the LHC. A comprehensive set of production and decay measurements are combined. The decays to $\gamma\gamma$, ZZ, WW, $\tau\tau$, and bb pairs are exploited, including studies targeting Higgs bosons produced in association with a pair of top quarks. The data samples were collected in 2011 and 2012 and correspond to integrated luminosities of up to 5.1 fb^{-1} at 7 TeV and up to 19.7 fb^{-1} at 8 TeV; the final detector calibration and alignment are used in the event reconstruction. From the high-resolution $\gamma\gamma$ and ZZ channels, the mass of this Higgs boson is measured to be $125.03\,^{+0.26}_{-0.27}\,(\text{stat.})\,^{+0.13}_{-0.15}\,(\text{syst.})$ GeV, with the precision dominated by the statistical uncertainty. For this mass, the event yields obtained in the different analyses tagging specific decay modes and production mechanisms are consistent with those expected for the standard model Higgs boson. The combined best-fit signal strength, relative to the standard model expectation, is found to be $1.00 \pm 0.09\,(\text{stat.})\,^{+0.08}_{-0.07}\,(\text{theo.}) \pm 0.07\,(\text{syst.})$ at the measured mass. Various searches for deviations in the magnitudes of the Higgs boson scalar couplings from those predicted for the standard model are performed. No significant deviations are found.

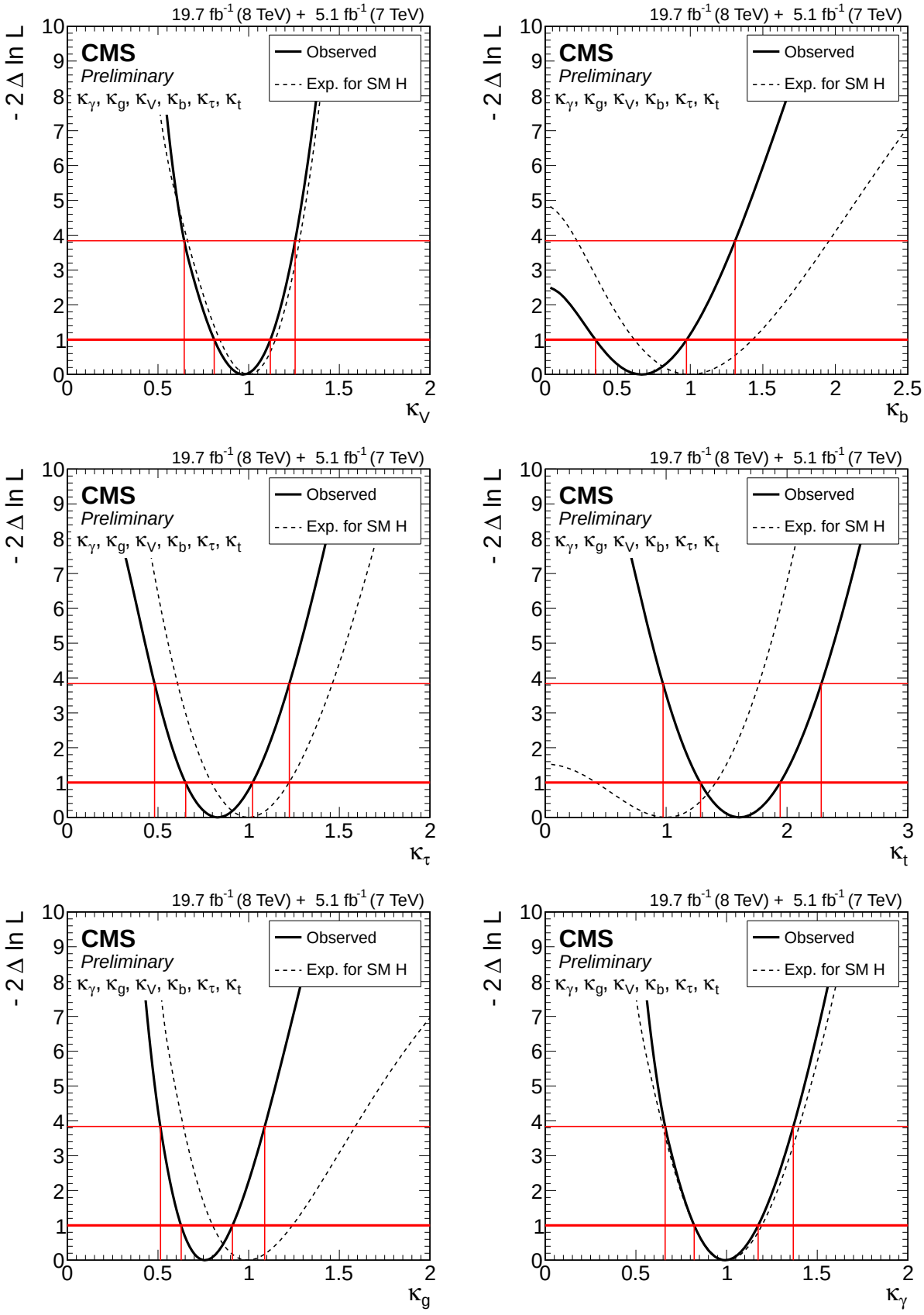

Figure 13: Likelihood scans for the model with six coupling scaling factors, one coupling at a time while profiling the remaining five together with all other nuisance parameters; from left to right and top to bottom: κ_V, κ_b, κ_τ, κ_t, κ_g, and κ_γ.

Table 5: Tests of the compatibility of the data with the SM Higgs boson couplings. The best-fit values and 68% and 95% CL confidence intervals are given for the evaluated scaling factors κ_i or ratios $\lambda_{ij} = \kappa_i/\kappa_j$. The different compatibility tests discussed in the text are separated by horizontal lines. When one of the scaling factors in a group is evaluated, others are treated as nuisance parameters.

Model		Best-fit result			Comment
Parameters	Table in Ref. [27]	Parameter	68% CL	95% CL	
κ_Z, λ_{WZ} (κ_f =1)	-	λ_{WZ}	$0.94^{+0.22}_{-0.18}$	[0.61,1.45]	$\lambda_{WZ} = \kappa_W/\kappa_Z$ using ZZ and 0/1-jet WW channels.
κ_Z, λ_{WZ}, κ_f	44 (top)	λ_{WZ}	$0.91^{+0.14}_{-0.12}$	[0.70,1.22]	$\lambda_{WZ} = \kappa_W/\kappa_Z$ from full combination.
κ_V, κ_f	43 (top)	κ_V	$1.01^{+0.07}_{-0.07}$	[0.88,1.15]	κ_V scales couplings to W and Z bosons.
		κ_f	$0.89^{+0.14}_{-0.13}$	[0.64,1.16]	κ_f scales couplings to all fermions.
κ_g, κ_γ	48 (top)	κ_g	$0.89^{+0.10}_{-0.10}$	[0.69,1.10]	Effective couplings to gluons (g) and photons (γ).
		κ_γ	$1.15^{+0.13}_{-0.13}$	[0.89,1.42]	
κ_g, κ_γ, BR_{BSM}	48 (middle)	BR_{BSM}	≤ 0.13	[0.00,0.32]	Branching fraction for BSM decays.
κ_V, λ_{du}, κ_u	46 (top)	λ_{du}	$1.01^{+0.20}_{-0.19}$	[0.66,1.43]	$\lambda_{du} = \kappa_u/\kappa_d$, relating up-type and down-type fermions.
κ_V, $\lambda_{\ell q}$, κ_q	47 (top)	$\lambda_{\ell q}$	$1.02^{+0.22}_{-0.21}$	[0.61,1.49]	$\lambda_{\ell q} = \kappa_\ell/\kappa_q$, relating leptons and quarks.
κ_g, κ_γ, κ_V, κ_b, κ_τ, κ_t	Similar to 50 (top)	κ_g	$0.76^{+0.15}_{-0.13}$	[0.51,1.09]	
		κ_γ	$0.99^{+0.18}_{-0.17}$	[0.66,1.37]	
		κ_V	$0.97^{+0.15}_{-0.16}$	[0.64,1.26]	
		κ_b	$0.67^{+0.31}_{-0.32}$	[0.00,1.31]	Down-type quarks (via b).
		κ_τ	$0.83^{+0.19}_{-0.18}$	[0.48,1.22]	Charged leptons (via τ).
		κ_t	$1.61^{+0.33}_{-0.32}$	[0.97,2.28]	Up-type quarks (via t).
as above plus BR_{BSM} and $\kappa_V \leq 1$	-	BR_{BSM}	≤ 0.34	[0.00,0.58]	

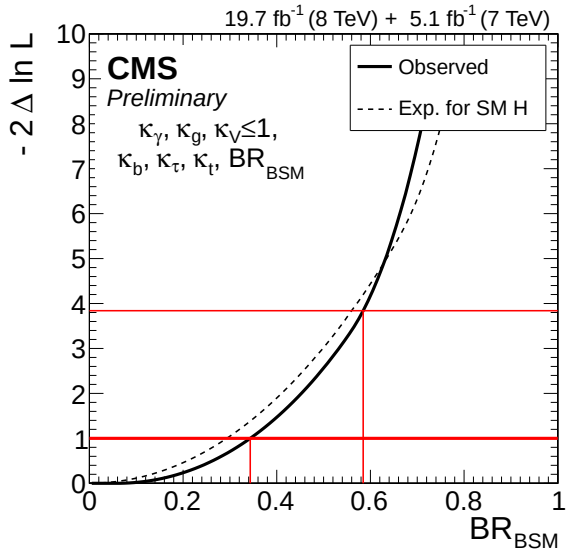

Figure 14: The likelihood scan versus $\mathrm{BR}_{\mathrm{BSM}} = \Gamma_{\mathrm{BSM}}/\Gamma_{\mathrm{tot}}$. The solid curve represents the observation in data and the dashed curve indicates the expected median results in the presence of the SM Higgs boson. The modifiers for both the tree-level and loop-induced couplings are profiled, but the couplings to the electroweak bosons are assumed to be bound by the SM expectation ($\kappa_{\mathrm{V}} \leq 1$).

References

[1] S. L. Glashow, "Partial-symmetries of weak interactions", *Nucl. Phys.* **22** (1961) 579, doi:10.1016/0029-5582(61)90469-2.

[2] S. Weinberg, "A model of leptons", *Phys. Rev. Lett.* **19** (1967) 1264, doi:10.1103/PhysRevLett.19.1264.

[3] A. Salam, "Weak and electromagnetic interactions", in *Elementary particle physics: relativistic groups and analyticity*, N. Svartholm, ed., p. 367. Almqvist & Wiskell, 1968. Proceedings of the 8th Nobel symposium.

[4] F. Englert and R. Brout, "Broken symmetry and the mass of gauge vector mesons", *Phys. Rev. Lett.* **13** (1964) 321, doi:10.1103/PhysRevLett.13.321.

[5] P. W. Higgs, "Broken symmetries, massless particles and gauge fields", *Phys. Lett.* **12** (1964) 132, doi:10.1016/0031-9163(64)91136-9.

[6] P. W. Higgs, "Broken symmetries and the masses of gauge bosons", *Phys. Rev. Lett.* **13** (1964) 508, doi:10.1103/PhysRevLett.13.508.

[7] G. S. Guralnik, C. R. Hagen, and T. W. B. Kibble, "Global conservation laws and massless particles", *Phys. Rev. Lett.* **13** (1964) 585, doi:10.1103/PhysRevLett.13.585.

[8] P. W. Higgs, "Spontaneous symmetry breakdown without massless bosons", *Phys. Rev.* **145** (1966) 1156, doi:10.1103/PhysRev.145.1156.

[9] T. W. B. Kibble, "Symmetry breaking in non-Abelian gauge theories", *Phys. Rev.* **155** (1967) 1554, doi:10.1103/PhysRev.155.1554.

[10] ATLAS Collaboration, "Observation of a new particle in the search for the standard model Higgs boson with the ATLAS detector at the LHC", *Phys. Lett. B* **716** (2012) 1, doi:10.1016/j.physletb.2012.08.020, arXiv:1207.7214.

[11] CMS Collaboration, "Observation of a new boson at a mass of 125 GeV with the CMS experiment at the LHC", *Phys. Lett. B* **716** (2012) 30, doi:10.1016/j.physletb.2012.08.021, arXiv:1207.7235.

[12] CMS Collaboration, "Observation of a new boson with mass near 125 GeV in pp collisions at $\sqrt{s}$ = 7 and 8 TeV", *JHEP* **06** (2013) 081, doi:10.1007/JHEP06(2013)081, arXiv:1303.4571.

[13] ATLAS Collaboration, "Measurement of the Higgs boson mass from the $H \to \gamma\gamma$ and $H \to ZZ^* \to 4\ell$ channels with the ATLAS detector using 25 fb^{-1} of pp collision data", (2014). arXiv:1406.3827. Submitted for publication in Phys. Rev. D.

[14] CMS Collaboration, "Search for the standard model Higgs boson produced in association with a top-quark pair in pp collisions at the LHC", *JHEP* **05** (2013) 145, doi:10.1007/JHEP05(2013)145, arXiv:1303.0763.

[15] ATLAS Collaboration, "Measurements of Higgs boson production and couplings in diboson final states with the ATLAS detector at the LHC", *Phys. Lett. B* **726** (2013) 88, doi:10.1016/j.physletb.2013.08.010, arXiv:1307.1427.

[16] CMS Collaboration, "Search for the standard model Higgs boson produced in association with a W or a Z boson and decaying to bottom quarks", *Phys. Rev. D* **89** (2014) 012003, doi:10.1103/PhysRevD.89.012003, arXiv:1310.3687.

[17] CMS Collaboration, "Measurement of Higgs boson production and properties in the WW decay channel with leptonic final states", *JHEP* **01** (2014) 096, doi:10.1007/JHEP01(2014)096, arXiv:1312.1129.

[18] CMS Collaboration, "Measurement of the properties of a Higgs boson in the four-lepton final state", *Phys. Rev. D* **89** (2014) 092007, doi:10.1103/PhysRevD.89.092007, arXiv:1312.5353.

[19] CMS Collaboration, "Evidence for the 125 GeV Higgs boson decaying to a pair of τ leptons", *JHEP* **05** (2014) 104, doi:10.1007/JHEP05(2014)104, arXiv:1401.5041.

[20] CMS Collaboration, "Observation of the diphoton decay of the 125 GeV Higgs boson and measurement of its properties", CMS-HIG-13-001, CERN-PH-EP-2014-117, 2014. Submitted for publication in Eur. Phys. J. C.

[21] CMS Collaboration, "Search for a Higgs boson decaying into a Z and a photon in pp collisions at $\sqrt{s} = 7$ and 8 TeV", *Phys. Lett. B* **726** (2013) 587, doi:10.1016/j.physletb.2013.09.057, arXiv:1307.5515.

[22] ATLAS Collaboration, "Search for Higgs boson decays to a photon and a Z boson in pp collisions at $\sqrt{s} = 7$ and 8 TeV with the ATLAS detector", *Phys. Lett. B* **732** (2014) 8, doi:10.1016/j.physletb.2014.03.015, arXiv:1402.3051.

[23] ATLAS Collaboration, "Search for Invisible Decays of a Higgs Boson Produced in Association with a Z Boson in ATLAS", *Phys. Rev. Lett.* **112** (2014) 201802, doi:10.1103/PhysRevLett.112.201802, arXiv:1402.3244.

[24] CMS Collaboration, "Search for invisible decays of Higgs bosons in the vector boson fusion and associated ZH production modes", (2014). arXiv:1404.1344. Submitted for publication in Eur. Phys. J. C.

[25] CMS Collaboration, "Study of the mass and spin-parity of the Higgs boson candidate via its decays to Z boson pairs", *Phys. Rev. Lett.* **110** (2013) 081803, doi:10.1103/PhysRevLett.110.081803, arXiv:1212.6639.

[26] ATLAS Collaboration, "Evidence for the spin-0 nature of the Higgs boson using ATLAS data", *Phys. Lett. B* **726** (2013) 120, doi:10.1016/j.physletb.2013.08.026, arXiv:1307.1432.

[27] LHC Higgs Cross Section Working Group, "Handbook of LHC Higgs Cross Sections: 3. Higgs Properties", (2013). arXiv:1307.1347.

[28] CMS Collaboration, "Search for Higgs Boson Production in Association with a Top-Quark Pair and Decaying to Bottom Quarks or Tau Leptons", Technical Report CMS-PAS-HIG-13-019, CERN, Geneva, 2013.

[29] CMS Collaboration, "Search for the standard model Higgs boson produced in association with top quarks in multilepton final states", Technical Report CMS-PAS-HIG-13-020, CERN, Geneva, 2013.

[30] CMS Collaboration, "Evidence for the direct decay of the 125 GeV Higgs boson to fermions", *Nat. Phys.* **advance online publication** (2014) doi:10.1038/nphys3005, arXiv:1401.6527.

[31] CMS Collaboration, "The CMS experiment at the CERN LHC", *JINST* **3** (2008) S08004, doi:10.1088/1748-0221/3/08/S08004.

[32] ATLAS and CMS Collaborations, LHC Higgs Combination Group, "Procedure for the LHC Higgs boson search combination in Summer 2011", Technical Report ATL-PHYS-PUB 2011-11, CMS NOTE 2011/005, 2011.

[33] CMS Collaboration, "Combined results of searches for the standard model Higgs boson in pp collisions at $\sqrt{s} = 7$ TeV", *Phys. Lett. B* **710** (2012) 26, doi:10.1016/j.physletb.2012.02.064, arXiv:1202.1488.

[34] G. Cowan, K. Cranmer, E. Gross, and O. Vitells, "Asymptotic formulae for likelihood-based tests of new physics", *Eur. Phys. J. C* **71** (2011) 1554, doi:10.1140/epjc/s10052-011-1554-0, arXiv:1007.1727.

[35] L. Moneta et al., "The RooStats Project", in *13th International Workshop on Advanced Computing and Analysis Techniques in Physics Research (ACAT2010)*. SISSA, 2010. arXiv:1009.1003. PoS(ACAT2010)057.

[36] B. Efron, "Bootstrap methods: another look at the jackknife", *Ann. Statist.* **7** (1979) 1, doi:10.1214/aos/1176344552. See "Remark K".

[37] S. M. S. Lee and G. A. Young, "Parametric bootstrapping with nuisance parameters", *Statist. Probab. Lett.* **71** (2005) 143, doi:10.1016/j.spl.2004.10.026.

[38] L. D. Landau, "On the angular momentum of a two-photon system", *Dokl. Akad. Nauk* **60** (1948) 207.

[39] C. N. Yang, "Selection rules for the dematerialization of a particle into two photons", *Phys. Rev.* **77** (1950) 242, doi:10.1103/PhysRev.77.242.

[40] M. J. G. Veltman, "Limit on mass differences in the Weinberg model", *Nucl. Phys. B* **123** (1977) 89, doi:10.1016/0550-3213(77)90342-X.

[41] P. Sikivie, L. Susskind, M. B. Voloshin, and V. I. Zakharov, "Isospin breaking in technicolor models", *Nucl. Phys. B* **173** (1980) 189, doi:10.1016/0550-3213(80)90214-X.